PHYSICAL REVIEW D **87,** 094013 (2013)

Three-prong distribution of massive narrow QCD jets

Matan Field,[1] Guy Gur-Ari,[2] David A. Kosower,[3] Lorenzo Mannelli,[2] and Gilad Perez[2,4]

[1]*Harish-Chandra Research Institute, Chhatnag Road, Jhusi, Allahabad 211019, India*

[2]*Department of Particle Physics and Astrophysics, Weizmann Institute of Science, Rehovot 76100, Israel*

[3]*Institut de Physique Théorique, CEA-Saclay, F-91191 Gif-sur-Yvette cedex, France*

[4]*CERN Physics Department, Theory Division, CH-1211 Geneva 23, Switzerland*

(Received 28 January 2013; published 13 May 2013)

We study the planar-flow distributions of narrow, highly boosted, massive QCD jets. Using the factorization properties of QCD in the collinear limit, we compute the planar-flow jet function from the one-to-three splitting function at tree level. We derive the leading-log behavior of the jet function analytically. We also compare our semianalytic jet function with parton-shower predictions using various generators.

DOI: 10.1103/PhysRevD.87.094013 PACS numbers: 12.38.−t

I. INTRODUCTION

Observables sensitive to the substructure of energetic, ultramassive jets hold great promise for distinguishing new physics signals from QCD backgrounds. Both the ATLAS and CMS experiments are pursuing studies relying on such observables in various new-physics searches [1,2] (see also Refs. [3–5] for an earlier search by the CDF collaboration). Boosted jets originating from electroweak gauge bosons [6], top quarks [7,8], Higgs bosons [9], and even new physics particles [10,11] are all of interest as targets of searches by the Tevatron and the LHC experiments. It is therefore important to be able to distinguish them from QCD jets. Recent reviews on substructure techniques, experimental status, and new-physics searches include Refs. [12–16] and references therein.

One way to characterize jet substructure is to consider observables which are functions of the energy flow within the jet, namely the energy distribution as measured by the detector (see Ref. [17] for a recent systematic classification). In this work we consider the hadronic collision

$$H_A + H_B \to J(\mathcal{O}; p_T, \eta; R) + X, \tag{1}$$

where H_A, H_B are the initial hadrons, and J is a jet with momentum given by p_T and η, with size R determined by the jet algorithm, and characterized by an energy-flow observable $\mathcal{O}$ such as the jet mass m. Note that $\mathcal{O}$ can stand for multiple energy-flow observables. We focus on narrow, highly boosted jets, and consider the inclusive differential QCD cross section for this process,

$$\frac{d\sigma_{2\to JX}(R)}{dp_T d\eta d\mathcal{O}}. \tag{2}$$

Such cross sections are usually computed using parton-shower codes, which offer much less insight into results than analytic computations. They also require significant computational resources.

In this article we follow a different approach, based on the collinear factorization properties of amplitudes in perturbative, massless QCD. Factorization allows us to focus on a single jet, ignoring to leading order the rest of the process, and to compute the differential jet substructure distribution semianalytically. In some limiting cases, we can compute the distribution completely analytically. As we demonstrate below, this method becomes useful when analyzing jets with sufficiently high p_T ($p_T \gtrsim 1$ TeV), a window recently opened at the LHC (see for example Refs. [1,2]).

There are various ways to define jet shapes. In the context of new-physics searches, a particularly useful way to characterize jet shape and substructure observables is by the first nontrivial order at which they appear in fixed-order perturbation theory [17–19]. Consider, for instance, Higgs boson searches: at leading order the Higgs boson decays to two partons with large invariant mass. The relevant nontrivial substructure observables must distinguish two-prong jets from the broad spectrum of all jets. Given a Higgs-boson mass and p_T, its decay kinematics are fully determined by one additional continuous variable, such as the ratio between the two decay-product momenta [9] or the opening angle between them [18]. The first nontrivial QCD background arises from corrections in which the jet is made up of two partons. If the Higgs boson recoils against a jet, this background first arises at next-to-leading order in two-jet production, when $2 \to 3$ processes are taken into account. This contribution is of $\mathcal{O}(\alpha_s^3)$ in fixed-order perturbation theory.

In this example, the signal distribution at fixed p_T is fully characterized by the jet mass and jet angularity [18,20]. We may think of these two quantities as replacing partonic (and therefore unphysical) parameters with physical infrared- and collinear-safe jet-shape observables [18]. When working to leading order (LO) in the jet mass, the angularity distribution is the only independent jet-shape observable that can separate the signal from the background. The corresponding leading order distribution, given a mass cut, can be computed analytically both for the signal and background [18], using the collinear approximation, which is adequate for narrow massive jets. The difference between the signal and background

distributions turns out to be modest, because both the QCD and Higgs-boson angularity distributions are monotonically decreasing functions between identical limiting values of the angularity variable. The same result obtains when considering the ratio of momenta or other kinematical variables, because they are all fully correlated with the angularity distribution. The similarity of the bounds on both the signal and background does yield a sharp prediction of this apparently naive picture. This prediction was qualitatively verified experimentally in the CDF collaboration's study [5] of high-p_{T} massive jets.

The next example of interest involves studies of high-p_{T} top quarks. At leading order, each top quark decays to three partons; in the decay, each parton pair typically has a large invariant mass. The same configuration is also relevant to studies of new physics [7,8], for example of gluino decay in R-parity violating scenarios [21]. A useful jet-shape observable in such a study is the planar flow [18,22,23]. If we focus on studying one top quark out of the produced pair, the leading QCD background is two-jet production where we constrain one of the jets to have a significant planar flow. This background first arises at next-to-next-to-leading order in two-jet production, when $2 \to 4$ processes are taken into account. The contribution is of $\mathcal{O}(\alpha_s^4)$ in fixed-order perturbation theory.

While the planar-flow distribution of a top-quark jet at leading order can be computed straightforwardly from its known matrix element, the planar-flow distribution of the QCD background has not yet been computed for narrow massive jets. The corresponding distribution was presented in Ref. [5] with a rather limited sample size due to the limited statistics of massive boosted jets at the Tevatron. LHC experiments have collected a much larger number of massive jets, which should allow a more precise measurement of the planar-flow distribution.

Our main purpose in this article is to compute the planar-flow distribution of narrow massive jets to leading order in QCD. We use the collinear approximation, in which we approximate the matrix element for such jets by $1 \to 3$ collinear splitting functions. Motivated by boosted-top studies, we take the jet mass to be roughly the top-quark mass. Our approximation is relevant when the jet p_{T} is substantially larger than the jet mass; we take the p_{T} to be $\mathcal{O}(1\ \mathrm{TeV})$. Our computation assumes a jet algorithm that produces approximately circular jets with radius R in the pseudorapidity–azimuthal angle plane, but is otherwise general. The use of the collinear approximation also requires that the jet radius not be too large; we take $R = 0.4$. In parton-shower simulations to which we compare, we use the anti-k_{T} algorithm, with the same jet size. As already mentioned, this year's $t\bar{t}$-resonance searches are already exploring this range of parameter space.

Jet shape observables can be viewed as moments of the energy distribution within a jet [17]. They are highly susceptible to contamination from pileup and other sources of soft radiation, especially for larger cone sizes [24,25]. Such contamination is a major concern at present, with more than 20 interactions on average at each LHC bunch crossing. This number is expected to grow even larger in future runs. Various techniques [24,26] allow one to estimate and subtract pileup contributions. Approaches in which jet-substructure analyses and searches are done in a way which is inherently less susceptible to such contamination would offer desirable alternatives to contamination subtraction.

Two main classes of alternative approaches have emerged: "filtering" [9] (see also Ref. [27]) and "template overlap" [19]. In the former, a measured jet is declustered and its soft components are removed. This leaves only its hard components to be reclustered into the "filtered" reclustered jet. In the second approach measured jets are not manipulated, and are instead compared to a set of templates built according to a chosen (computed) fixed-order distribution of signal jets. The comparison makes use of an "overlap function" which evaluates the degree of overlap between each measured jet and the set of templates. The reader will find a discussion of jet-substructure observables and experimental applications in Refs. [28–31].

For both alternative approaches, it would be useful to study distributions of the core (hard) component of jets. This is relatively straightforward for the signals, but much more challenging for the QCD background. The semianalytic calculations we pursue here are a first step in this direction, as our results provide a semianalytic understanding of the kinematical distributions of the hard component of massive jets with nontrivial three-body kinematics. For this purpose we also compare the result of our full $1 \to 3$ calculation with a similar calculation employing an iterated $1 \to 2$ collinear splitting function in the approximation to the matrix element. We also discuss how various scale choices affect our result. Finally, we compare our results with parton-shower results, both with and without matching to tree-level matrix elements. We cross-check our calculations with a simple analytic expression for the planar-flow distribution in the small-planar-flow limit.

The paper is organized as follows. In Secs. II and III, we define the planar-flow observable, introduce narrow jets and discuss various aspects of calculations of the jet function. In Sec. IV, we relate the jet functions of narrow jets to collinear splitting functions for two-body jets. As an illustrative example we compute the leading-order jet function for the mass distribution using splitting functions. In Sec. IV B we prove that spin correlations in the splitting function factorize in all cases that are of interest in this article. In Sec. V we use these methods to compute the leading-order combined mass and planar-flow jet function of three-body jets. For small values of the planar flow we obtain an analytic result below, while at large planar flow we rely on numerical integration. We also compare the jet function to one computed using an iterated $1 \to 2$ approximation,

discuss the behavior of the jet function at large planar flow, and discuss the sensitivity to scale choices. In Sec. VI, we compare the semianalytic jet function to parton-shower calculations with and without matching to fixed-order matrix elements. We also discuss hadronization corrections, and corrections from terms in matrix elements beyond the collinear approximation. We present our conclusions in Sec. VII. Six appendices furnish a variety of technical details.

II. PLANAR FLOW

We are interested in two energy flow observables—the jet mass and planar flow. The jet mass squared is

$$\left(\sum_{i\in\text{jet}} p_i\right)^2, \tag{3}$$

where i refers here to any parton (or hadron or tower or topocluster in a more realistic experimental context) inside the jet. For a hadronic collider we may define the planar flow as follows. Define first a 2×2 momentum shape tensor,

$$\mathcal{I} \equiv \sum_{i\in\text{jet}} p_{\text{T}}^i \begin{pmatrix} \Delta\eta_i^2 & \Delta\eta_i\Delta\phi_i \\ \Delta\eta_i\Delta\phi_i & \Delta\phi_i^2 \end{pmatrix}, \tag{4}$$

where $(\Delta\eta_i, \Delta\phi_i) = (\eta_i - \eta_{\text{jet}}, \phi_i - \phi_{\text{jet}})$ are the pseudorapidity and azimuthal-angle difference of each jet constituent from the jet axis. We take all constituents to be massless. This form is manifestly boost invariant for boosts along the beam axis.

The planar flow (Pf) is then defined by

$$\text{Pf} \equiv \frac{4\det\mathcal{I}}{(\text{Tr}\,\mathcal{I})^2}. \tag{5}$$

One can easily verify that $0 \le \text{Pf} \le 1$, and that it vanishes for two-body jets, receiving its leading contribution from three-body jets.[1] The latter property means that the planar flow is potentially useful for distinguishing the QCD background from top jets. The value $\text{Pf} = 0$ arises when the partons lie on a line in the detector plane. In particular, it will vanish for three-body jets when a parton becomes soft, or when two partons become collinear. Three-parton configurations that are symmetric about the jet axis have $\text{Pf} = 1$. Configurations with n partons symmetric under rotations by $2\pi/n$ radians around the jet axis also have $\text{Pf} = 1$.

For the sake of convenience, in the theoretical calculations that follow we will focus on central jets (that is, with very small pseudorapidity). For such jets we can work in terms of the angles θ and ϕ (being the polar coordinates around the jet axis), set $\eta = 0$, and exchange p_{T} for p (the overall jet momentum). For narrow, central jets, we can rewrite the momentum-inertia tensor as follows:

$$\mathcal{I}^{kl} = \sum_{i\in\text{jet}} E_i \frac{p_{\perp,i,k}}{E_i}\frac{p_{\perp,i,l}}{E_i}, \quad k,l = 1,2, \tag{6}$$

where $p_{\perp,i,k}$ is the kth component of the transverse momentum of constituent i with respect to the jet axis.

As we review in Sec. IV, the leading-log behavior of the jet function for the jet mass is given by

$$J_f(m^2; p_{\text{T}}, R) \simeq \frac{\alpha_s \tilde{c}_f}{\pi}\frac{1}{m^2}\log\left(\frac{p_{\text{T}}^2R^2}{m^2}\right), \tag{7}$$

where in this case $\tilde{c}_g = C_A = 3$ and $\tilde{c}_q = C_F = 4/3$, and the jet radius $R = \sqrt{\Delta\eta^2 + \Delta\phi^2}$. In this article we compute the mass and planar-flow jet function at leading order in α_s, for narrow QCD jets. In the limit of small Pf we will obtain an analytic result for the leading-log behavior of the jet function. For small $m/p_{\text{T}}R$ it is given by the expression

$$J_f(m^2, \text{Pf}; p_{\text{T}}; R) = \frac{\alpha_s^2 c_f}{\pi^2}\cdot\frac{1}{m^2}\log\left(\frac{p_{\text{T}}^2R^2}{m^2}\right)\cdot\frac{1}{\text{Pf}}\log\left(\frac{1}{\text{Pf}}\right), \tag{8}$$

$$c_g = 2C_A^2, \qquad c_q = C_F(C_A + C_F). \tag{9}$$

Away from the limit of small planar flow, we will compute the planar-flow jet function semianalytically, using numerical integration to obtain the final result. We will show that there is a physically interesting regime of parameters, with the jet mass near the top-quark mass and with $0.4 \lesssim \text{Pf} \lesssim 0.95$, in which our result has rough agreement with the parton-shower simulations. (As shown below, the parton-shower results of different tools do not fully agree with each other, which however is not the focus of this study.) We expect our results to be useful for understanding how to refine methods to distinguish highly boosted top jets from the QCD background at the LHC.

The planar-flow distribution was measured by CDF [5] and ATLAS [3], but with large statistical uncertainties, and using too large a cone size and too big a mass-to-momentum ratio to be compared with our results. At the LHC, accurate measurements of planar-flow distributions are difficult due to pileup effects; but we may expect them to improve significantly over time. In principle, one can "refine" jets in a controlled manner (by applying filtering; by using the template overlap method and then looking at the parton distribution of the peak templates; by looking at events with a small number of vertices; or by using other methods for pileup subtraction), and thereby isolate the hard part of the measured jet in order to compare with theoretical predictions even in the presence of incoherent soft radiation.

III. NARROW MASSIVE JETS

Let us consider jets at the parton level. If we take a jet to be narrow ($R^2 \ll 1$), the partons will be approximately collinear. As we review in the next section, when massless

[1] Notice that because $\text{Tr}\,\mathcal{I}$ is proportional to the jet mass [26], the planar flow is only well defined for massive jets.

partons become collinear the QCD cross section factorizes partially, and we can write (schematically for now)

$$\frac{d\sigma_{2\to JX}(R)}{dp_{\mathrm{T}}d\eta d\mathcal{O}}\bigg|_{\mathcal{O}=\mathcal{O}_0} \simeq \sum_f \frac{d\sigma_{2\to fX}(R)}{dp_{\mathrm{T}}d\eta}\cdot J_f(\mathcal{O}_0; p_{\mathrm{T}}, \eta; R). \tag{10}$$

In the cross section on the right-hand side, the partons making up the jet are replaced by a parent parton of type f, which can be either a gluon or one of the massless quarks. The jet substructure is encoded in the jet function J_f, which has a simple physical interpretation: it is the probability distribution for the parent parton of type f to evolve into a jet of size R that has $\mathcal{O} = \mathcal{O}_0$. Accordingly, its integral is normalized to unity, $\int d\mathcal{O} J_f(\mathcal{O}) = 1$. Throughout our study we will be agnostic about the specific jet algorithm used in the analysis, and will assume only that it produces approximately circular jets with radius R in the η-ϕ plane.

As we review in the next section, at fixed order in α_s the jet function can be computed from splitting functions [32], universal functions that govern the behavior of the squared matrix element in the collinear limit. In this limit, the squared matrix element factors into a product of a splitting function and a squared matrix element with lower multiplicity. In general, the factorization is not complete, due to the dependence of the splitting functions on the spin of the parent parton. We will show, however, that for all energy-flow observables the spin dependence does factorize.

The fixed-order splitting function is singular in the limit where partons become soft or collinear. In Eq. (10) this singularity appears as a divergence of the jet function in the infrared limit of the observable $\mathcal{O}$ (for example taking $m \to 0$ in a two-body jet). Resumming higher-order (perturbative) corrections cures the divergence, and replaces it with a peak at a finite value of $\mathcal{O}$ (for reviews see for example Refs. [33–36]). A fixed-order calculation is accordingly unreliable when we get close to the infrared limit. This problem can be avoided by considering only values of the observable $\mathcal{O}$ that are far away from the infrared limit, compared with the peak position in its distribution. In particular, we will always take the jet mass to be "large enough" in this sense. The peak in the jet-mass distribution, m_{peak}, is roughly near its average at $m_{\mathrm{ave}} = \alpha_s p_{\mathrm{T}} R$ [12], and we will take our jet mass to be much larger, $m \gg m_{\mathrm{peak}}$, where we expect the fixed-order perturbative calculation to be reliable.

Beyond higher-order perturbative corrections requiring resummation, there are also nonperturbative corrections (in the form of hadronization), which become important in the infrared and tend to smear the jet function. If some of the fixed-order partons have transverse momentum relative to the jet that is small compared to the characteristic transverse momentum of the smearing effect, the final jet function will be dominated by the latter effects. Keeping the observable $\mathcal{O}$ away from its infrared limit avoids this problem as well. On the other hand, in order for the collinear approximation to hold, we cannot stray too far from the infrared limit. Finally, in order for the approximated distribution (in the collinear limit and at fixed order in α_s) to be valid, we should not get too close to kinematic boundaries.

For our approximation to be reliable, we need a range of values for $\mathcal{O}$ that obeys these constraints. Applying the constraints to the jet-mass observable, and requiring that we have a nonempty range of validity for the approximation, necessitates considering jets with sufficiently high p_{T}. We therefore consider only highly boosted jets. For a general observable, the existence of such a range of validity is less clear. We will show later that to reasonable accuracy, a nontrivial range of validity does indeed exist for the mass and planar-flow jet functions with collision parameters typical of the LHC.

IV. QCD JET-MASS DISTRIBUTION IN THE COLLINEAR LIMIT

In this section we compute the jet-mass distribution for massless QCD in the collinear limit using the splitting function [32], for both quark and gluon jets. Consider again the hadronic collision,

$$H_A(q_A) + H_B(q_B) \to J(\mathcal{O}; p_{\mathrm{T}}, \eta; R) + X, \tag{11}$$

where H_A, H_B are the initial hadrons with momenta q_A, q_B, and J is a jet of cone size R and given p_{T} and η. The jet is further characterized by an energy-flow observable $\mathcal{O}$. For simplicity, in this section we will take $\mathcal{O}$ to be the jet mass squared, m^2; in the next section we will consider also the planar flow.

The factorized cross section is given by

$$\frac{d\sigma_{H_AH_B\to JX}(R)}{dp_{\mathrm{T}}d\eta dm^2} = \sum_{f_A,f_B}\int dx_A dx_B \phi_{f_A}(x_A)\phi_{f_B}(x_B) \times \frac{d\sigma_{f_Af_B\to JX}}{dp_{\mathrm{T}}d\eta dm^2}(x_A, x_B, p_{\mathrm{T}}, \eta, m; R), \tag{12}$$

where ϕ_{f_A}, ϕ_{f_B} are the parton distribution functions. For narrow jets $d\sigma_{f_Af_B\to JX}$ further factorizes at leading order into a jet function, times a cross section in which the jet is replaced by a single parent parton,

$$\frac{d\sigma_{f_Af_B\to JX}}{dp_{\mathrm{T}}d\eta dm^2}(x_A, x_B, p_{\mathrm{T}}, \eta, m; R) \simeq \sum_f \frac{d\sigma_{f_Af_B\to fX}}{dp_{\mathrm{T}}d\eta}(x_A, x_B, p_{\mathrm{T}}, \eta) J_f(m; p_{\mathrm{T}}, \eta; R). \tag{13}$$

The sum is over the type f of the parent parton, which can be a gluon or a quark with a specific flavor. The relation (13) is due to the factorization of the QCD matrix element

in the limit where two or more partons become collinear. The universal function in the factorization is proportional to the splitting function. We therefore seek to express the jet function in terms of the splitting function.

A. Quark jets

Let us first consider the case where the parent parton is a quark. This case is simpler because the quark splitting function does not depend on the helicity of the parent parton. Here the cross section factorizes completely in the collinear limit. Consider the matrix element for the scattering of two into n massless QCD partons,

$$\mathcal{M}_{2\to n} \equiv \mathcal{M}^{c_1,\ldots,c_{n+2};s_1,\ldots,s_{n+2}}_{f_1,\ldots,f_{n+2}}(p_1,\ldots,p_{n+2}). \tag{14}$$

Here p_i denote parton momenta; the f_i, parton types; the c_i, their colors; and the s_i, their helicities. Outgoing particles are indexed by $i = 1,\ldots,n$, and incoming particles by $i = n+1,\ n+2$. Define the abbreviation $|\mathcal{M}_{2\to n}|^2 \equiv |\mathcal{M}_{f_1,\ldots,f_{n+2}}(p_1,\ldots,p_{n+2})|^2$ for the squared matrix element summed over color and helicities (averaged in the case of incoming particles—we will leave this distinction implicit from now on).

Consider the limit in which two outgoing partons, say p_1 and p_2, become collinear. The leading contribution to $|\mathcal{M}_{2\to n}|^2$ in this limit is from diagrams in which the two outgoing partons originate from a single parent parton with momentum $p = p_1 + p_2$, and with a type f that is uniquely determined by the splitting process $f \to f_1 f_2$. In the collinear limit the parent goes on shell, leading to a $1/p^2$ singularity. When the parent is a quark, the squared matrix element factorizes as we approach the limit,

$$|\mathcal{M}_{f_1,f_2,f_3,\ldots,f_{n+2}}(p_1,p_2,p_3,\ldots,p_{n+2})|^2 \simeq |\mathcal{M}_{f,f_3,\ldots,f_{n+2}}(p,p_3,\ldots,p_{n+2})|^2 \cdot \frac{8\pi\alpha_s}{s_{12}} P_{f_1f_2}(p_1,p_2), \tag{15}$$

where $s_{12} \equiv (p_1+p_2)^2$, and $P_{f_1f_2}$ is the spin-averaged splitting function [32,37], given in Appendix A. In the squared matrix element on the right-hand side, the two collinear partons are replaced by their parent parton. For a gluon jet, the splitting function depends on the helicity of the parent parton, and the factorization is not as simple as in Eq. (15); we consider this case in the next subsection.

The fixed-order differential cross section is given in terms of the squared matrix element [38],

$$d\hat{\sigma}_{2\to n} = \frac{1}{8E_{n+1}E_{n+2}} \prod_{i=1}^{n}\left[\frac{1}{2E_i}\frac{d^3p_i}{(2\pi)^3}\right] |\mathcal{M}_{2\to n}|^2 \times \delta^4(p_{\mathrm{f,tot}} - p_{\mathrm{i,tot}}). \tag{16}$$

Using Eq. (15) and making a change of variables $(\vec{p}_1,\vec{p}_2) \to (\vec{p}_1,\vec{p} = \vec{p}_1+\vec{p}_2)$, it is easy to see that near the collinear limit,

$$d\hat{\sigma}_{2\to n} \simeq d\hat{\sigma}_{2\to n-1} \times \frac{4\pi\alpha_s}{s_{12}} \frac{E}{E_1E_2} \frac{d^3p_1}{(2\pi)^3} \times P_{f_1f_2}(p_1,p_2)|_{\vec{p}_2=\vec{p}-\vec{p}_1}, \tag{17}$$

where $d\hat{\sigma}_{2\to n-1}$ is defined in terms of the matrix element on the right-hand side of Eq. (15). Comparing with the postulated relation (13), we may now write down the jet function,

$$J_f(m^2;\vec{p};R) = \frac{\alpha_s E}{2\pi^2 m^2} \sum_{f\to f_1f_2} \frac{1}{S_{f_1f_2}} \times \int \frac{d^3p_1 d^3p_2}{E_1E_2} \delta^3(\vec{p}_1+\vec{p}_2-\vec{p}) P_{f_1f_2}(p_1,p_2) \times \delta(m^2(p_1,p_2)-m^2)\Theta(R-\theta_1)\Theta(R-\theta_2). \tag{18}$$

Here, θ_i are the angles of the momenta $\vec{p}_i$ with respect to the jet axis $\vec{p}$, and the step functions $\Theta(R-\theta_i)$ are put in by hand to enforce[2] a cone of size R. The sum is over allowed splitting processes, and the symmetry factor $S_{f_1f_2}$ corrects the overcounting of identical parton configurations in Eq. (18): it is 2 when $f_1 = f_2$, and 1 when they are different. We stress that Eq. (18) is valid only to leading order in α_s at the partonic level. The full jet function receives corrections at higher orders in perturbation theory (some of which require resummation) as well as from nonperturbative effects.

It is now a straightforward exercise to substitute the quark splitting function into Eq. (18) and compute the jet function, assuming $R \ll 1$. The quark splitting function is [32,37]

$$P_{q\to gq}(z) = C_F \frac{1+(1-z)^2}{z}, \tag{19}$$

where $C_F = (N_c^2-1)/2N_c$, and $z = E_g/E$ is the emitted gluon's energy fraction, in our approximation. Using Eq. (19) and solving the integral in Eq. (18), we find the leading-log expression for the quark jet function, valid for $m \ll pR$,

$$J_q(m^2;p;R) \simeq \frac{C_F\alpha_s}{\pi}\frac{1}{m^2}\log\left(\frac{p^2R^2}{m^2}\right). \tag{20}$$

This result was derived in Ref. [22] using slightly different terminology but a similar limit. As we explain in detail in Appendix F, the form of Eq. (20) can be alternatively obtained by rewriting the mass as a function of the emission angle and z, and replacing z with m as the integration variable. This makes explicit the overall $1/m^2$ dependence, and the integration over the angle within the allowed kinematical boundaries further leads to the log in Eq. (20).

[2]This procedure is expected to be compatible, up to higher-order corrections in R, with any jet algorithm that produces approximately circular jets [18].

When $m \to 0$, the jet function (20) diverges. This is an infrared divergence, resulting from partons becoming soft and collinear. In this limit higher order contributions in α_s become important, and after resumming them the singularity is exponentially suppressed. Thus, the full jet function vanishes in the massless jet limit (see for example Refs. [33–36]); and because it decays at large mass, a peak of the jet mass is expected to arise at low jet mass. The result in Eq. (20) is therefore only reliable when $m_{\text{peak}} \ll m \ll pR$. The divergence in Eq. (20) also renders the distribution non-normalizable. Nevertheless, in the regime where our approximation is valid we expect our result to match the full jet function including its overall normalization. In other words, in this regime it gives the (leading) probability distribution of a quark to evolve into a radius-R jet with mass m [18,22]. This behavior was verified experimentally, at least qualitatively, in Ref. [5].

B. Gluon jets

We now turn to the case of gluon jets. Unlike the quark case, the gluon splitting functions have a nontrivial dependence on the helicity of the parent parton. As a result, the collinear factorization of the squared matrix element is incomplete. For the computation of the jet-mass distribution, the incomplete factorization does not alter the leading-log result: in this case, the spin correlations are nonsingular. However, we would like to go beyond this and establish a general result that will be useful in the rest of our study. The spin correlations always factorize when one considers distributions of energy-flow observables defined for a single jet. We will prove this for the $1 \to 2$ splitting function, and the proof can be easily generalized to the $1 \to 3$ splitting function.

In the presence of spin correlations, the collinear factorization (15) of the squared matrix element is no longer correct, and instead we have [37]

$$|\mathcal{M}_{f_1,f_2,f_3,\ldots,f_{n+2}}(p_1, p_2, p_3, \ldots, p_{n+2})|^2 \simeq \frac{8\pi\alpha_s}{s_{12}} \sum_{ss'} \mathcal{T}^{ss'}_{f,f_3,\ldots,f_{n+2}}(p, p_3, \ldots, p_{n+2}) \hat{P}^{ss'}_{f_1 f_2}(p_1, p_2), \tag{21}$$

where now $\hat{P}$ is the helicity-dependent splitting function, and $\mathcal{T}$ is defined in terms of the matrix element $\mathcal{M}_{2\to n-1}$ by

$$\mathcal{T}^{s_1 s_1'}_{f_1,\ldots,f_{n+1}}(p_1, \ldots, p_{n+1}) \equiv \sum_{\substack{s_2,\ldots,s_{n+1} \\ c_1,c_2,\ldots,c_{n+1}}} \mathcal{M}^{c_1,\ldots,c_{n+1};s_1,\ldots,s_{n+1}}_{f_1,\ldots,f_{n+1}}(p_1, \ldots, p_{n+1}) \times [\mathcal{M}^{c_1,\ldots,c_{n+1};s_1',\ldots,s_{n+1}}_{f_1,\ldots,f_{n+1}}(p_1, \ldots, p_{n+1})]^\dagger. \tag{22}$$

$\mathcal{T}$ is essentially the matrix element $\mathcal{M}_{2\to n-1}$, squared, except that there is no sum over the helicity of the jet's parent parton.

The differential cross section no longer factorizes as it did in Eq. (17). However, in the jet-function definition the phase-space integral includes an azimuthal integral around the jet axis. For example, changing the integration variables in Eq. (18) to polar coordinates (p_i, θ_i, ϕ_i), $i = 1, 2$ (relative to the jet axis $\vec{p}$), the integration over rotations around the jet axis is described by the variable $\phi \equiv \phi_1$, keeping $(\phi_2 - \phi_1)$ fixed. Therefore, for any observable that is invariant under rotations around the jet axis, the integral picks out the part of the splitting function that is invariant under such rotations, which is precisely the spin-averaged splitting function. This includes all energy-flow observables defined in terms of a single jet, because for such observables there is no preferred direction in the detector plane that can break the rotational symmetry. We may therefore replace $\hat{P}^{ss'} \to \delta^{ss'} P$, where P is the spin-averaged splitting function. Noting that $\mathcal{T}^{ss'}\delta^{ss'} = |M_{2\to n-1}|^2$, the rest of the computation follows through as in the previous section, and we conclude that the jet function for gluon jets is given by Eq. (18), just as for quark jets.

We conclude this section by computing the leading-log part of the gluon jet-mass function. For $R^2 \ll 1$ and $m^2 \ll (pR)^2$, the leading contribution comes only from the $g \to gg$ splitting function,

$$P_{gg}(z) = 2C_A\left[\frac{z}{1-z} + \frac{1-z}{z} + z(1-z)\right], \tag{23}$$

where $C_A = N_c$, and we find

$$J_g(m^2; p; R) \simeq \frac{C_A\alpha_s}{\pi}\frac{1}{m^2}\log\left(\frac{p^2R^2}{m^2}\right), \tag{24}$$

again in agreement with Ref. [22].

V. PLANAR-FLOW JET FUNCTION

In this section we compute the planar-flow jet function $J_f(m^2, \text{Pf}; p_T; R)$, which receives its leading contribution from three-body jets. This jet function factorizes from the rest of the cross section when we take the "triple" collinear limit, in which three partons become collinear simultaneously. The limit is analogous to the ("double") collinear limit that we studied in the last section.

We consider $2 \to n$ scattering with matrix element $\mathcal{M}$, where three outgoing massless partons with four-momenta p_1, p_2, p_3 are collinear. The parton energies are denoted by E_i. The jet made out of these three partons has energy $E = \sum_{i=1}^3 E_i$, momentum p and mass m. Finally, we define the energy fractions $z_i \equiv E_i/E$, and also

$$s_{ij} \equiv (p_i + p_j)^2 = 2p_i \cdot p_j, \quad i, j = 1, 2, 3, \qquad s_{123} \equiv (p_1 + p_2 + p_3)^2 = m^2. \tag{25}$$

In the collinear limit, the squared matrix element of the scattering process factorizes as follows [37]:

$$|\mathcal{M}_{f_1,f_2,f_3,\ldots,f_{n+2}}(p_1,p_2,p_3,\ldots,p_{n+2})|^2 \simeq \frac{64\pi^2\alpha_s^2}{s_{123}^2}\mathcal{T}^{ss'}_{f,f_4,\ldots,f_{n+2}}(p,p_4,\ldots,p_{n+2})\hat{P}^{ss'}_{f_1f_2f_3}(p_1,p_2,p_3). \quad (26)$$

Here, $\hat{P}^{ss'}_{f_1f_2f_3}$ is the one-to-three splitting function [37,39] for the splitting $f \to f_1f_2f_3$; the type f of the parent parton is determined by flavor conservation. The splitting function depends on the outgoing momenta and each parton f_i is associated to a momentum p_i. As in Sec. IV B, performing the azimuthal-angle integrals will make spin correlations disappear in the jet function. We may thus replace $\mathcal{T}^{ss'}\hat{P}^{ss'}_{f_1f_2f_3}$ by $|M_{2\to n-1}|^2 P_{f_1f_2f_3}$, where $P_{f_1f_2f_3}$ is the spin-averaged splitting function. In the jet function we will need to sum over all possible final partons and, as before, take into account the symmetry factor that compensates for an overcounting of identical-parton configurations. Let us define then

$$P_f \equiv \sum_{f\to f_1f_2f_3}\frac{1}{S_{f_1f_2f_3}}P_{f_1f_2f_3}, \quad (27)$$

where $S_{f_1f_2f_3}$ equals $n!$ for a parton configuration that includes n identical partons. Accordingly,

$$P_g = \frac{1}{3!}P_{ggg} + N_f P_{gq\bar{q}}, \quad (28)$$

$$P_q = \frac{1}{2!}P_{ggq} + \frac{1}{2!}P_{qq\bar{q}} + (N_f-1)P_{\bar{Q}Qq}, \quad (29)$$

where Q denotes a quark with a different flavor than that of the parent q. The spin-averaged splitting functions $P_{f_1f_2f_3}$ are given in Appendix B.

The jet function is given by a straightforward generalization of Eq. (18),

$$J_f(m^2,\mathrm{Pf};\vec{p};R) \simeq \frac{\alpha_s(m)\alpha_s(\mu)E}{4\pi^4m^4}\int\prod_{i=1}^{3}\left[\frac{d^3p_i}{E_i}\Theta(R-\theta_i)\right] \times P_f(\vec{p}_i)\delta(m^2(\vec{p}_i)-m^2) \times \delta(\mathrm{Pf}(\vec{p}_i)-\mathrm{Pf})\delta^3\left(\vec{p}-\sum\vec{p}_i\right). \quad (30)$$

As discussed in detail further below (see Sec. V E), the two strong-coupling factors are evaluated at different scales[3]: we take the first scale to be m, corresponding to the first $1\to 2$ splitting, and we choose the second scale to approximate that of the second splitting according to an ordering scheme defined below (obviously for "Mercedes"-like configurations the ordering does not make a difference).

An equivalent definition of the jet function (30) is provided by averaging the splitting function over parton permutations,

$$P_f \to \tilde{P}_f \equiv \frac{1}{6}\sum_{\sigma\in S_3}P_f(p_{\sigma(1)},p_{\sigma(2)},p_{\sigma(3)}), \quad (31)$$

while restricting the integration domain to

$$\int_{-\infty}^{\infty}d^3p_1d^3p_2d^3p_3 \to 3\int_{E_1<E_2,E_3}d^3p_1d^3p_2d^3p_3. \quad (32)$$

The motivation for this alternative formulation will become clear below, but the basic idea will be to keep one parton (say, $\vec{p}_3$) away from its soft limit $E_3\to 0$. We can do this without loss of generality as our jet is assumed to be of a large mass.

Let us now integrate over $\vec{p}_3$ in Eq. (30) by using momentum conservation. In the remaining integral let us switch to spherical coordinates relative to the jet axis $\vec{p}$, (p_i,θ_i,ϕ_i), $i=1,2$.

Next, we extract the leading-order expressions for the integrand in the narrow-jet expansion $\theta_i < R \ll 1$. The resulting expressions appear in Appendix C. Using these, as well as the explicit splitting functions, one may easily check that the integrand in Eq. (30) depends on the azimuthal angles ϕ_i only through the combination $\cos(\phi_1-\phi_2)$. We make the change of variables $\int_0^{2\pi}d\phi_1d\phi_2 f(\cos(\phi_1-\phi_2)) = 4\pi\int_0^{\pi}d\phi f(\cos(\phi))$.

We can now write the jet function as follows:

$$J_f \simeq \frac{3\alpha_s^2 p}{\pi^3m^4}\int_0^R d\theta_1d\theta_2\int_0^{\pi}d\phi\int_{\mathcal{C}}dp_1dp_2\frac{p_1p_2\theta_1\theta_2}{p_3} \times \tilde{P}_f(\vec{p}_i)\delta(m^2(\vec{p}_i)-m^2)\delta(\mathrm{Pf}(\vec{p}_i)-\mathrm{Pf}), \quad (33)$$

where the domain of integration is

$$\mathcal{C} \equiv \{(p_1,p_2)|0\le p_1\le p_2,\, p_3,\, \theta_3\le R\}. \quad (34)$$

Here, p_3 and θ_3 are given (in terms of our integration variables) by Eqs. (C4) and (C5), respectively. It can be easily seen that the resulting collinear expansion of p_3, Eq. (C5), breaks down for small p_3. In other words, the soft limit of p_3 and the collinear limit do not commute. Therefore, one cannot use the expansion (C5) in the vicinity of small p_3. We avoid this complication by formulating the jet function in a way that avoids that part of the integration region, as in Eq. (32).

Using Eq. (C5), the inequality $\theta_3\le R$ is equivalent at leading order to

$$p\left(R^2-\frac{m^2}{p^2}\right) - p_1(R^2-\theta_1^2) - p_2(R^2-\theta_2^2) \ge 0. \quad (35)$$

Notice that we need $m < pR$ to have a nonvanishing domain, in accordance with the narrow jet approximation. Very close to the kinematic boundary the leading contribution

[3]For the sake of brevity we allow ourselves to be sloppy in our notation: generally μ in Eq. (30) depends on the parton configuration in the integrand, so $\alpha_s(\mu)$ should really appear inside the integral.

will be dominated by higher order terms; consequently, we must require m to be safely away from the kinematic boundary, $m^2 \ll (pR)^2$.

Before proceeding, let us discuss the expected range of validity of our theoretical computation. Take $p_T \simeq p = 1$ TeV. The collinear approximation requires that $R^2 \ll 1$; we choose $R = 0.4$ for our analyses, the same as the smallest cone size used at the LHC for new-physics searches. As for the jet mass, we would like to stay well below the kinematic boundary at pR, but also well above the peak in the mass distribution (very roughly at $\alpha_s pR$), so that higher-order effects in α_s remain small. We choose $m \simeq 180$ GeV, which satisfies both of these constraints. This choice is also well motivated physically, as it is close to the top-quark mass. The singularity at small Pf would be eliminated by resummation of higher powers of log Pf; we would expect such a resummation to lead to a Sudakov-like exponential damping term, $\sim \exp(-\log^2 \mathrm{Pf})$, similar to the case of the thrust or jet-mass distribution [40]. To the best of our knowledge no computation of this effect has been carried out to date. In any case the focus of our present investigation is on massive jets with sizable planar flow where higher-order corrections, resummed or not, have a subdominant impact. Qualitatively, we expect the Pf distribution to be similar to that of the jet mass, namely, vanishing for Pf $= 0$, peaking at a small value of Pf, and falling gradually beyond that point. As we shall see in Sec. VI, the jet parameters chosen above lead to a Sudakov peak in the planar-flow distribution near Pf $=$ 0.1. We will not restrict the range of planar-flow values in our discussion, but remind the reader that physically reliable results are expected within our framework only for planar-flow values well above this peak.

A. Analytic leading-log behavior

In this section we compute the jet function analytically in the limit of small planar flow and at fixed jet mass. For simplicity, we will take the second running scale μ in Eq. (30) equal to the first, m. We will find that the leading-log result, in the limit of small Pf and small m/pR, is given by Eq. (8).

At Pf $= 0$, the integral in Eq. (33) diverges because the splitting function is singular. The singularity arises in regions of integration where a parton becomes soft, or two partons become collinear (with respect to the third parton). In fact, the leading singularity in the integrand arises in the combined soft-collinear limit, where a single parton becomes both soft and collinear with another parton. In the splitting functions (see Appendix B), the terms responsible for this leading singularity are those proportional[4] to $(s_{ij}z_i)^{-1}$ or $(s_{ij}s_{ik})^{-1}$.

At small (but nonzero) Pf, the leading contribution to the (finite) integral will thus come from the soft-collinear regions, which are disconnected in the domain of integration. In Eq. (33) there are two such regions, where parton 1 is soft, and collinear with either parton 2 or 3. Because of the symmetry of the partons, it suffices to compute the contribution from one region. We will compute the contribution from the region in which parton 1 is soft ($p_1 \to 0$), and collinear with parton 2 ($\theta_{12} \to 0$).

Let us choose more convenient variables in Eq. (33) to describe the collinear limit,

$$\theta_1 = \theta, \qquad \theta_2 = \theta(1 + r\cos\omega), \qquad \phi = r\sin\omega. \tag{36}$$

To leading order in r, we see from Eq. (C6) that $\theta_{12} = \theta r$, and the collinear limit is now parametrized by $r \to 0$.

In the soft-collinear limit ($p_1, r \to 0$) the splitting function can be written as

$$\tilde{P}_f = \frac{F_f(\theta; p, m)}{p_1^2 r^2} + \cdots, \tag{37}$$

where the dots include less singular terms; this is the leading singularity to which we alluded above. The functions F_f are given by

$$F_g = 2\frac{C_F T_R N_f m^2 p^2\theta^2(m^4 + p^4\theta^4) + C_A^2(m^4 + m^2p^2\theta^2 + p^4\theta^4)^2}{3p^2\theta^4(m^2 + p^2\theta^2)^2}, \tag{38}$$

$$F_q = C_F\frac{2C_F m^6 + (C_A + 2C_F)m^4p^2\theta^2 + (2C_A + C_F)m^2p^4\theta^4 + 2C_A p^6\theta^6}{3p^2\theta^4(m^2 + p^2\theta^2)}. \tag{39}$$

As we seek the leading Pf $\to 0$ singularity, we will include only these terms in the splitting function.

Using Eqs. (C5), (C9), and (C10), at leading order in p_1, r and in the collinear approximation we have

$$m^2 = \frac{p^2p_2\theta^2}{p - p_2}, \qquad \mathrm{Pf} = \frac{4p^3p_1p_2\theta^4r^2\sin^2\omega}{m^4(p - p_2)}, \qquad p_3 = p - p_2. \tag{40}$$

[4]One might have expected terms proportional to s_{ij}^{-2} to lead to an even higher singularity. A careful examination of these terms, though, reveals that they are in fact less singular than the other ones mentioned above.

The integration domain (34) becomes[5]

$$\mathcal{C} \simeq \left\{(p_1, p_2)|p_1 \geq 0, (R^2 - \theta^2)p_2 \leq p\left(R^2 - \frac{m^2}{p^2}\right)\right\}. \quad (41)$$

The jet function (33) can now be written as

$$J_f \simeq \frac{6\alpha_s^2 p}{\pi^3 m^4} \int_0^R d\theta \int_0^\pi d\omega \int_{\mathcal{C}} dp_1 dp_2 \times \int_0^{r^{\max}} dr \frac{p_1 p_2 \theta^3 r}{p - p_2} \delta\left[\frac{p^2 p_2 \theta^2}{p - p_2} - m^2\right] \times \delta\left[\frac{4p^3 p_1 p_2 \theta^4 r^2 \sin^2\omega}{m^4(p - p_2)} - \mathrm{Pf}\right] \tilde{P}_f(\vec{p}_i), \quad (42)$$

with a factor of 2 from the sum over the soft-collinear regions. The upper integration limit for r is a function of the other variables whose precise form is irrelevant to the leading behavior we are trying to compute.

In the limit of small planar flow, the dominant contribution to the jet function is from the integration region near the soft-collinear singularity. We may therefore restrict our domain of integration to a small region around the singularity, defined by

$$0 < p_1 < p_1^{\max}, \qquad 0 < r < r^{\max}, \quad (43)$$

where now both $r^{\max}$ and $p_1^{\max}$ are chosen constant and small. We expect that, in the small Pf limit, the jet function will not depend on these parameters. Indeed, we will see that $r^{\max}$ and $p_1^{\max}$ will drop out of the result.

We can now solve the delta functions for p_1 and p_2,

$$p_1 = \frac{m^2 \mathrm{Pf}}{4p\theta^2 r^2 \sin^2\omega}, \qquad p_2 = \frac{m^2 p}{m^2 + p^2\theta^2}. \quad (44)$$

Taking into account the Jacobian and the appropriate domain, we find

$$J_f \simeq \frac{6\alpha_s^2 p^2}{\pi^3 m^2 \mathrm{Pf}} \int_{m^2/p^2 R}^R d\theta \frac{\theta^3 F_f(\theta; p, m)}{(m^2 + p^2\theta^2)^2} \times \int_0^\pi d\omega \int_{\frac{m}{\theta \sin\omega}\sqrt{\frac{\mathrm{Pf}}{4pp_1^{\max}}}}^{r^{\max}} \frac{dr}{r}, \quad (45)$$

where the lower integration limit on r emerges from the previous upper integration limit on p_1. Proceeding with the r integration, we finally find the leading-log approximation for the jet function,

$$J_f \simeq \frac{A_f}{\mathrm{Pf}} \log\left(\frac{1}{\mathrm{Pf}}\right) + \cdots, \quad (46)$$

where

$$A_f \equiv \frac{3\alpha_s^2 p^2}{\pi^2 m^2} \int_{m^2/p^2 R}^R d\theta \frac{\theta^3 F_f(\theta, p, m)}{(p^2\theta^2 + m^2)^2}. \quad (47)$$

As anticipated, the arbitrary integration limits $r^{\max}$ and $p_1^{\max}$ do not appear in the leading term. When we include the first correction, the jet function takes the form

$$J_f \simeq \frac{A_f}{\mathrm{Pf}} \log\left(\frac{B_f}{\mathrm{Pf}}\right) + \cdots \quad (48)$$

Here we will not compute B_f, which does depend on the values of $r^{\max}$ and $p_1^{\max}$. The remaining integral in Eq. (47) can be performed analytically, and the full result is given in Appendix D. Here we record only the result to leading order in m/pR,

$$A_f \simeq \frac{\alpha_s^2 c_f}{\pi^2} \frac{1}{m^2} \log\left(\frac{p^2 R^2}{m^2}\right), \quad (49)$$

where $c_g = 2C_A^2$, $c_q = C_F(C_A + C_F)$. This is the same leading-log behavior that we found in the case of the jet-mass function.

For the relevant range of parameters as taken earlier, the contributions subleading in m/pR cannot be neglected. Taking $p = 1$ TeV, $m = 180$ GeV, $R = 0.4$, and evaluating the coupling at the jet mass scale, we find $A_g = 0.683\ \mathrm{TeV}^{-2}$, $A_q = 0.227\,\mathrm{TeV}^{-2}$. In the next section we will compare this result with a full semianalytic evaluation of the jet function in the collinear approximation.

In Appendix F we show how, in parallel to the evaluation of the jet-mass distribution, the most singular term in the jet-Pf distribution can be obtained simply by iterating the $1 \to 2$ splitting function. The $1/\mathrm{Pf}$ factor arises from changing variables for the second emission-energy fraction while the log (Pf) factor results from integrating the angular variable within the kinematic constraints.

B. Semianalytic evaluation

Let us now return to the expression (33) for the jet function, and proceed without making further assumptions. We will carry out two integrations using the delta function constraints, and compute the remaining integrals numerically to obtain the jet function. This computation is valid in the collinear approximation and for any planar flow.

Let us perform the integration in Eq. (33) over p_1 and p_2 by using the mass and planar-flow constraints. Solving these constraints, one finds two solution branches $p_i^{\pm}$ that should be summed over,

$$p_1^{(\pm)}(\theta_1, \theta_2, \phi) = \frac{2m^2 p^3 \theta_1^2 \theta_2^2 \sin^2\phi + m^4 p \mathrm{Pf}\,\theta_2(\theta_2 - \theta_1\cos\phi) \pm \sqrt{\Delta}}{4p^2\theta_1^2\theta_2^2\sin^2\phi(m^2 + p^2\theta_1^2) + m^4 \mathrm{Pf}(\theta_1^2 + \theta_2^2 - 2\theta_1\theta_2\cos\phi)}, \quad (50)$$

[5]As we are interested only in the region where p_1 is soft, $p_1 \leq p_2$, p_3 is automatically satisfied at a fixed mass.

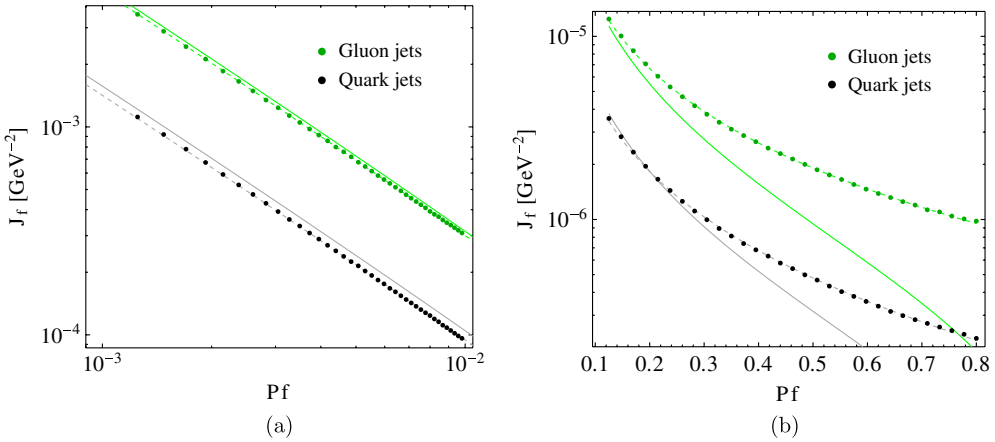

FIG. 1 (color online). Comparison of semianalytic jet functions (dots) with the purely analytic leading-log form of Eq. (48) (solid lines) and with a fit to the leading-log form (dashed lines). The quark functions are the lower (black) curves and the gluon ones are the upper (green) curves. Two ranges of the planar-flow observable are shown: (a) $10^{-3} < \mathrm{Pf} < 10^{-2}$ and (b) $0.1 < \mathrm{Pf} < 0.8$. The curve parameters are listed in Table I; the purely analytic parameters are given in column 1, the fit parameters for (a) in column 2, and the fit parameters for (b) in column 3. In the purely analytic form, A_f is given by Eq. (49), and $B_f = 1$. In the fit to the leading-log form, A_f is determined by fitting in both (a) and (b), while $B_f = 1$ is set to 1 in (a) and is determined by fitting in (b). The jet momentum is $p = 1$ TeV, with mass $m = 180$ GeV and size $R = 0.4$.

$$p_2^{(\pm)}(\theta_1, \theta_2, \phi) = p_1^{(\mp)}(\theta_2, \theta_1, \phi), \tag{51}$$

where

$$\Delta \equiv m^4 p^2 \theta_1^2 \theta_2^2 \sin^2\phi \{2p^2\theta_1\theta_2[p^2\theta_1\theta_2(1-\cos(2\phi)-2\mathrm{Pf}) - 2m^2\mathrm{Pf}\cos\phi] - m^4\mathrm{Pf}^2\}. \tag{52}$$

The jet function becomes

$$J_f \simeq \frac{6\alpha_s^2 p}{\pi^3 m^4} \sum_{s\in\{+,-\}} \int_{\mathcal{C}_s'} d\theta_1 d\theta_2 d\phi \frac{p_1^{(s)} p_2^{(s)} \theta_1 \theta_2}{p_3} |\mathcal{J}^{(s)}| \tilde{P}_f(\vec{p}_i), \tag{53}$$

where $\mathcal{J}^{(s)} = \partial(p_1^{(s)}, p_2^{(s)})/\partial(\mathrm{Pf}, m^2)$ is the Jacobian, and the new integration domain (including a reality condition for $p_i^{(\pm)}$) is

$$\mathcal{C}_s' = \{(\theta_1, \theta_2, \phi) | \Delta \geq 0, \quad 0 \leq p_1^{(s)} \leq p_2^{(s)}, p_3(p_i^{(s)}, \theta_i, \phi), \quad 0 \leq \theta_{1,2} \leq R, \quad 0 \leq \phi \leq \pi, \quad \theta_3(p_i^{(s)}, \theta_i, \phi) \leq R\}. \tag{54}$$

We compute the integral in Eq. (53) numerically.[6] For the comparison with the analytic result we take both couplings at the jet-mass scale; when comparing with the parton-shower simulations we take the first coupling at the jet-mass and the second coupling at the dipole scale (see Sec. V E and Appendix E). Figure 1 shows the results, including a fit to the predicted leading-log behavior. Table I compares the leading-log coefficients predicted in Sec. V A with those extracted from the fit. At planar-flow values below 10^{-2} we find good agreement with the predicted leading-log behavior. At larger values of the planar flow the subleading behavior becomes important, and the fit must include the subleading coefficient B_f as well. We stress that in the small-Pf region, higher-order effects are very important, so that the planar-flow jet function obtained here requires resummation and cannot be compared usefully with experimental data. Above $\mathrm{Pf} = 10^{-1}$ the leading coefficient A_f no longer agrees with the analytic prediction, which assumes $\mathrm{Pf} \ll 1$, but the jet function does match the general form in Eq. (48). In this region, we must integrate the splitting functions numerically to obtain a semianalytic prediction.

C. Comparison with iterated $1 \to 2$ splittings

In this section we obtain a different semianalytic approximation to the jet function, by approximating each $1 \to 3$ splitting function by an iteration of two $1 \to 2$ splitting functions. For simplicity, we ignore spin correlations, which do not contribute at leading order in small Pf.[7] This corresponds to the strongly ordered limit for the two splittings.

Consider again the squared matrix element

$$|M_{2\to n}|^2 = |M_{f_1 f_2 f_2 \ldots f_{n+2}}(p_1, p_2, p_3, \ldots, p_{n+2})|^2. \tag{55}$$

In the limit where p_1 and p_2 are collinear, that is have relative transverse momentum small compared to all other parton pairs, the matrix element (55) factorizes [cf. Eq. (15)] as

[6]We obtained all semianalytic results in this paper using MATHEMATICA with adaptive Monte Carlo integration.

[7]The $1 \to 3$ and $(1 \to 2)^2$ splitting functions can be shown to have the same soft-collinear leading singularity.

TABLE I. Fit coefficients for the leading-log form in Eq. (48). The coefficients A_f are in units of TeV^{-2}, where the B_f are dimensionless. The analytic result is only for the leading-order term (in small Pf), so that effectively $B_f = 1$.

	Analytic	Fit at small Pf	Fit at large Pf
A_g	0.683	0.651	0.413
A_q	0.227	0.205	0.138
B_g	1	Fixed to 1	5.06
B_q	1	Fixed to 1	2.85

$$|M_{2\to n}|^2 \simeq |M_{f',f_3,\ldots,f_{n+2}}(p', p_3, \ldots, p_{n+2})|^2 \cdot \frac{8\pi\alpha_s}{s_{12}} \times P_{f_1 f_2}(p_1, p_2), \tag{56}$$

where p' denotes the parent parton of partons 1 and 2, namely $p' = p_1 + p_2$, and f' is determined by f_1 and f_2. The splitting functions $P_{f_1 f_2}$ are given in Appendix A. Next, assume that p' and p_3 are also collinear, with relative transverse momentum small compared to that of remaining parton pairs (but large compared to that of p_1 and p_2). We then have the further factorization,

$$|M_{2\to n}|^2 \simeq |M_{f,f_4,\ldots,f_{n+2}}(p, p_4, \ldots, p_{n+2})|^2 \cdot \frac{64\pi^2\alpha_s^2}{s_{12}s_{123}} \times P_{f_1 f_2}(p_1, p_2) P_{f' f_3}(p', p_3), \tag{57}$$

where p and f are the jet's momentum and type, respectively. Comparing with Eq. (26), we can read off the iterated $1 \to 2$ approximation to the function P_f defined in Eq. (27),

$$P_f^{(1\to 2)^2} = \frac{s_{123}}{s_{12}} \sum_{f\to f' f_3 \to f_1 f_2 f_3} \frac{1}{S_{f_1 f_2}} P_{f' f_3}(p', p_3) P_{f_1 f_2}(p_1, p_2). \tag{58}$$

Explicitly,

$$P_g^{(1\to 2)^2} = \frac{s_{123}}{s_{12}}\left[\frac{1}{2}P_{gg}(p', p_3)P_{gg}(p_1, p_2) + N_f P_{gg}(p', p_3)P_{q\bar{q}}(p_1, p_2) + 2N_f P_{q\bar{q}}(p', p_3)P_{qg}(p_1, p_2)\right], \tag{59}$$

$$P_q^{(1\to 2)^2} = \frac{s_{123}}{s_{12}}\left[P_{qg}(p', p_3)P_{qg}(p_1, p_2) + \frac{1}{2}P_{gq}(p', p_3)P_{gg}(p_1, p_2) + N_f P_{gq}(p', p_3)P_{q\bar{q}}(p_1, p_2)\right]. \tag{60}$$

The strongly ordered approximation to the planar-flow jet function is given by Eq. (53), with $\tilde{P}_f$ replaced by $\tilde{P}_f^{(1\to 2)^2}$ [symmetrized over parton permutations—see Eq. (31)]. As in the case of the $1 \to 3$ splitting-function approximation to the planar-flow jet function, we may allow the argument scale of α_s to depend on the partonic configuration. We show the ratio of the jet functions in the strongly ordered approximation to those in the basic approximation of Sec. V B in Fig. 2, where the scales for all factors of the strong coupling are fixed to the jet mass m. The strongly ordered approximation giving rise to iterated $1 \to 2$ splittings implies a large hierarchy between the two splittings. This means it is valid in the limit of small Pf (keeping the mass fixed). We would thus expect the two jet functions to coincide in the small-Pf limit. In Fig. 2, the ratio does get closer to unity at small planar flow, but a gap appears to remain. This gap results from the discrete number of points chosen and the use of a linear scale; we have verified that it closes up when going further to very small Pf. In any event, a fixed-order calculation is not valid in this region; we should focus on the region $0.4 \lesssim \text{Pf} \lesssim 0.95$. In this latter region, which is relevant for physics

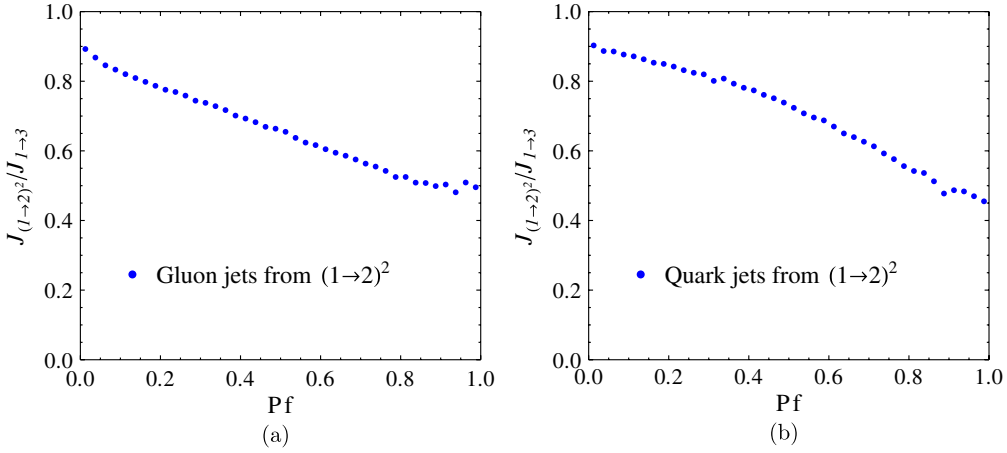

FIG. 2 (color online). The ratio of semianalytic jet functions evaluated with a splitting kernel approximated by an iterated $1 \to 2$ splittings, to those with the original $1 \to 3$ kernel. The parameters are $p = 1$ TeV, $m = 180$ GeV, and $R = 0.4$, and the couplings are evaluated at the jet-mass scale.

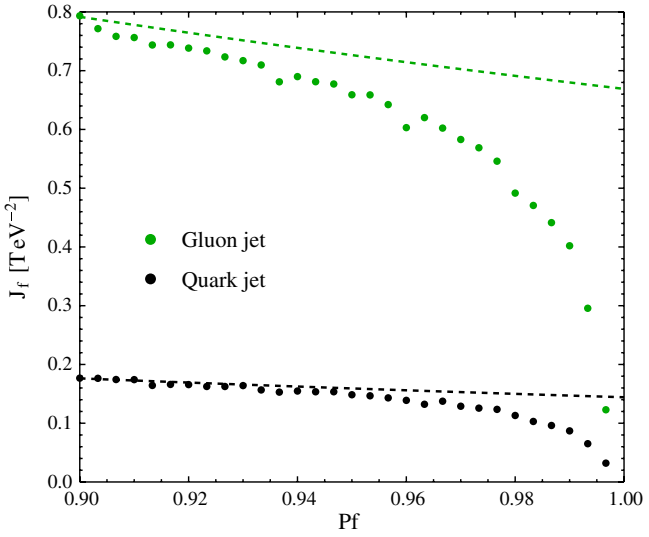

FIG. 3 (color online). Semianalytic jet function near Pf $= 1$. The dashed line shows the fit to the leading-log form of Eq. (48) with the coefficients given in Sec. V B.

searches related to top jets for instance, the difference between the two approximations is significant. In this region, the strongly ordered approximation fails to capture much of the essential physics. This has implications for parton-shower calculations of this quantity: we do not expect unmatched parton-shower calculations to be accurate. Matching to tree-level matrix elements—so long as it is done to a sufficiently high multiplicity as to ensure at least three matched partons inside a jet—will introduce the required corrections to the strongly ordered splitting functions. However, even the matched calculations may be quite sensitive to the matching procedure, and in particular to the size of the remaining region where the pure shower calculation is used.

D. Behavior at large planar flow

Coming back to the $1 \to 3$ computation (53), let us consider the jet function at Pf $= 1$. At this point

$$\Delta = -m^4 p^2 \theta_1^2 \theta_2^2 \sin^2\phi (m^2 + 2p^2\theta_1\theta_2\cos\phi)^2 \leq 0, \quad (61)$$

and we are within the integration domain only when $\Delta = 0$: the phase space dimension is reduced by 1. Because the splitting function has no singularities within this domain,[8] it implies that the jet function vanishes at Pf $= 1$ in our approximation.

Figure 3 confirms this by showing that the semianalytic jet function drops to zero as the planar flow approaches 1. As we will see below, the drop is a feature of our three-body approximation, and it will not be present when higher order corrections in α_s are included. It also shows the fit to the leading-log result, including the subleading coefficients in Eq. (48), and we notice that the semianalytic jet function diverges from the fit at the level of 10% near Pf $= 0.95$. We heuristically take this point to mark the beginning of the drop. Our three-body approximation is not valid beyond this point.

E. Comparison of running scales

In this section we consider how different choices of the running scale μ affect the jet function. Recall that the jet function (30) is of $\mathcal{O}(\alpha_s^2)$, and that we evaluate the two powers of α_s at different scales. One power we evaluate at the jet-mass scale (corresponding to the first $1 \to 2$ splitting in case of hierarchical emissions); but there are several possible choices of scale for the second power, corresponding to the second (softer) $1 \to 2$ splitting. We consider three possibilities:

(1) set μ to be the jet mass m,
(2) set $\mu = \min_{i,j}\{s_{ij}\}$, and
(3) set μ to be a hybrid scale, described by the $2 \to 3$ dipole scale for gluon emission or s_{ij} in the $g \to q\bar{q}$ case; see Appendix E for details.

We expect the last of these to be the most accurate one, and we compare the others against it in Fig. 4. The choice of scale makes a significant difference to the value of planar-flow jet function, of the order of 10%–30% at relevant values of the planar flow. Furthermore, the ratios are not constant as a function of the planar flow. A variation is to be expected in a leading-order calculation, as nothing in the matrix element compensates for the change of scale. We would expect this variation to be substantially smaller in a next-to-leading order calculation of the jet function. The scale variation is hidden in parton-shower calculations

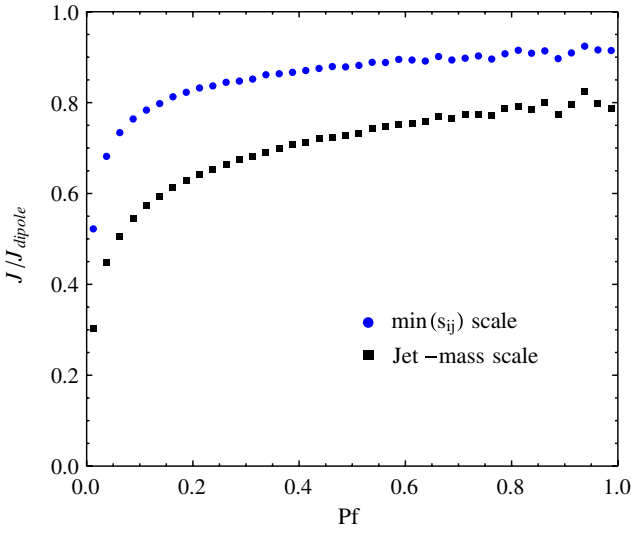

FIG. 4 (color online). Ratios of gluon jet functions with different choices for μ. The jet functions are evaluated at $p = 1$ TeV, $m = 180$ GeV, and $R = 0.4$, and they are divided by the jet function that uses the hybrid (dipole) scale.

[8]All splitting-function singularities come from soft or collinear limits, which imply Pf $\to 0$.

(as each algorithm chooses one particular scale), but this should be considered as an intrinsic source of uncertainty. Unlike the error made by applying a strongly ordered approximation, this uncertainty is not removed by matching to tree-level matrix elements. Matching to one-loop matrix elements as well would be required to reduce it.

The results displayed in Fig. 4 at large Pf can be understood in a simple way. At Pf = 1 we have a symmetric configuration of partons, where $s_{ij} = m^2/3$. Let us assume this is the dominant configuration. For a three-gluon configuration (which dominates the gluon jet function), the dipole scale is then $\mu_{\text{dipole}} = m/3$. We expect that the jet function ratios at Pf = 1 will be given by the corresponding ratios of couplings,

$$\frac{\alpha_s(\min(s_{ij}))}{\alpha_s(\mu^2_{\text{dipole}})} \approx 0.92, \qquad \frac{\alpha_s(m^2)}{\alpha_s(\mu^2_{\text{dipole}})} \approx 0.84. \tag{62}$$

This agrees nicely with Fig. 4, within numerical uncertainties.

VI. COMPARISON TO PARTON-SHOWER CODES

In this section we compare our semianalytic result to parton-shower simulations of QCD scattering at the LHC. The simulations are of $2 \to 4$ (matched) and $2 \to 2$ (unmatched) matrix-element scattering, plus showering. We used MADGRAPH/MADEVENT 5 [41] with PYTHIA 6.420 (virtual ordered) showering [42], and SHERPA 1.3.1 [43], and in both cases we have used the CTEQ6L set for the parton distribution function [44]. The jet algorithm is anti-k_T [45] with $R = 0.4$, implemented in FASTJET [46,47]. The other parameters are $\sqrt{s} = 7$ TeV, $950 < p_{\text{T}} < 1050$ GeV, and $|\eta| < 1$. We integrate over the mass window $160 < m < 200$ GeV, which is consistent with our motivation for this work. The simulations include showering but not hadronization or detector simulation. As we show below in Sec. VI A, the effect of hadronization at large planar flow is to increase the distribution by about 15%, while leaving the shape of the distribution unchanged.

The semianalytic results are computed at $p = 1$ TeV and integrated numerically over the same mass window. There are separate jet functions for gluon and quark jets, and the total jet function is given by $J = xJ_g + (1 - x)J_q$, where x can be thought of as the "fraction of gluon jets" in the sample. While this is not a well-defined quantity, we may get a rough estimate for it by considering matrix-element $2 \to 2$ scattering. Then x is given by the ratio of outgoing gluons to total outgoing partons (within the p_{T} and η cuts), and using this method we find $x \approx 0.24$.

The parton-shower distributions are normalized such that the integral of each over the full jet-mass and planar-flow ranges is 1. In particular, this means that the area under the plots presented below is *not* 1. Our jet functions are naturally normalized in the same way, so we expect the total jet function to agree with the parton-shower result within its range of validity.

Figure 5 shows the comparison of the semianalytic results to the parton-shower jet functions for MADGRAPH

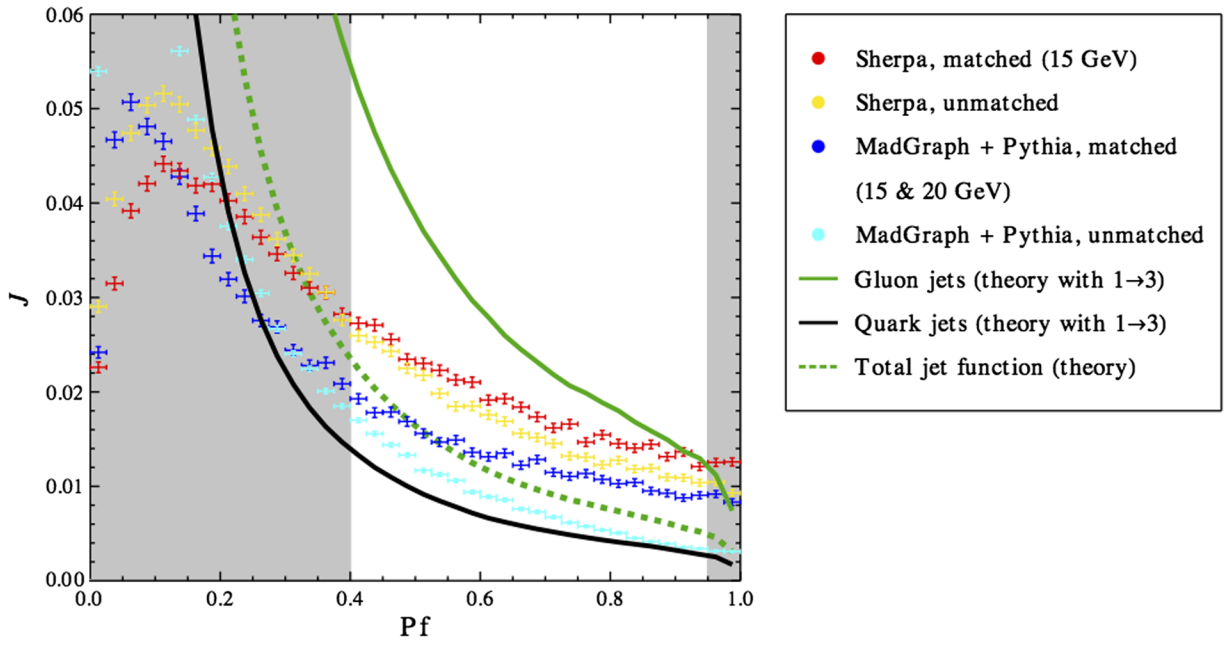

FIG. 5 (color online). Jet functions from parton-shower simulations, and our predictions of Sec. V B using $1 \to 3$ splitting functions for the quark and gluon planar-flow jet functions. The upper (green) solid curve shows the gluon jet function, and the lower (black) solid curve the quark one. The dashed (green) curve is the average jet function with gluon fraction $x = 0.24$. The region of expected validity of the semianalytic form is highlighted. The points with error bars show the parton-shower results, in the highlighted region from top to bottom: matched SHERPA (red), unmatched SHERPA (yellow), matched MADGRAPH (dark blue), and unmatched MADGRAPH (light blue).

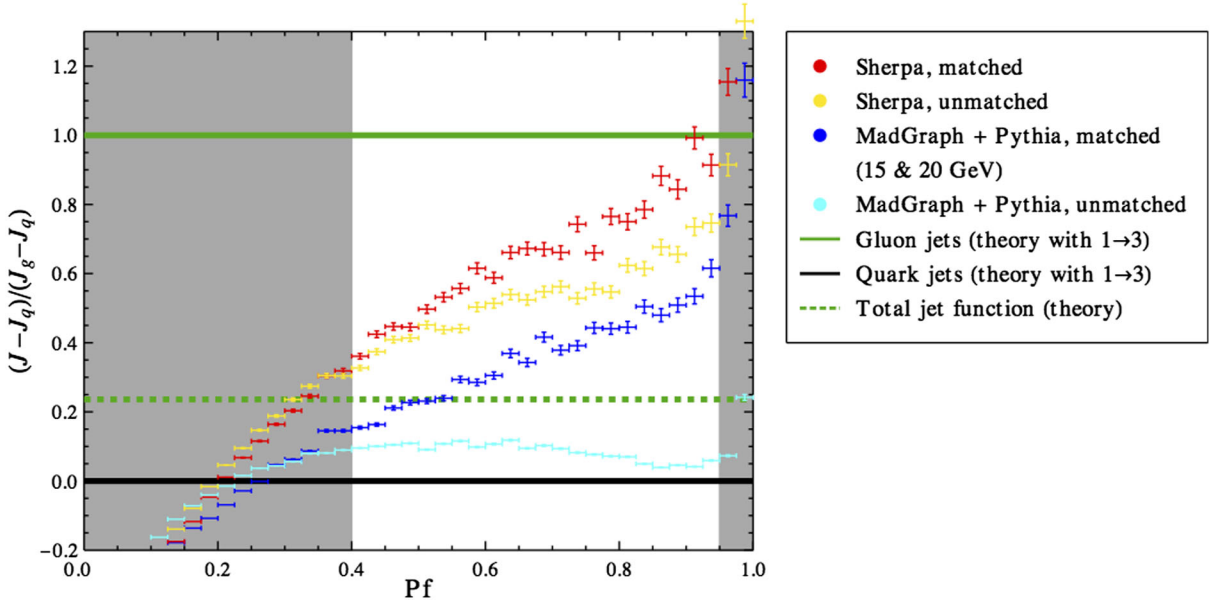

FIG. 6 (color online). Detailed comparison between jet functions from parton-shower simulations and our semianalytic results. The figure shows $(J - J_q)/(J_g - J_q)$, where J_g and J_q are respectively the semianalytic gluon and quark jet functions. These jet functions are shown by the upper (green) solid line at 1 and the lower (black) solid line at 0. The average jet function with gluon fraction $x = 0.24$ is shown by the dashed (green) line. The region of expected validity of the semianalytic form is highlighted. The points with error bars show the parton-shower results, with the order and color coding as in Fig. 5.

(with PYTHIA showering) and for SHERPA. The second factor of the strong coupling α_s is evaluated at the hybrid scale as described in Sec. V E. Away from the peak we find that the parton-shower results fall between the semianalytic quark and gluon functions, in agreement with the theoretical prediction. Notice that the parton-shower jet functions display no special behavior near Pf $= 1$, while our semianalytic jet functions drop to zero there (see Sec. V D). This discrepancy is due to missing higher-order contributions in the theoretical calculation. In detailed comparisons with our theoretical result we will exclude this highest-Pf region, restricting ourselves to the range Pf < 0.95.

The simulations include an infrared cutoff of 15 GeV at the matrix-element level, which represents the minimal k_T distance between pairs of partons.[9] A SHERPA simulation with a higher cutoff of 25 GeV (not shown in Fig. 5) gives a qualitatively similar result.

One can check, for example by generating random three-body jets, that a cutoff of 15 GeV implies the matrix-element results apply only at Pf $\gtrsim 0.4$. Below this only $1 \to 2$ splittings are in effect, and in addition we expect that resummation and nonperturbative effects become important. In support of this, below we will show that the effect of hadronization in the simulation does not alter the shape above Pf ≈ 0.4. On the theory side, as we approach the peak (at Pf ≈ 0.1) from above, resummation effects become important and our perturbative approximation breaks down. For the purpose of comparison we will therefore restrict ourselves to Pf $\gtrsim 0.4$.

Figure 6 shows a detailed comparison of the parton-shower and theoretical jet functions. The region in which we expect to find agreement is highlighted. Finally, Fig. 7 shows the comparison to the theoretical result using the iterated $1 \to 2$ splittings (see Sec. V C), with the second factor of the strong coupling α_s evaluated at the scale of the second splitting s_{ij}. Comparing with Fig. 5, it is clear that using the $1 \to 3$ splitting function results in a significantly better approximation to the jet function. (The first factors of the strong coupling α_s are evaluated at the jet-mass scale in both cases, but the choice of second scale is different.)

A. Hadronization

The effect of turning on hadronization in the parton-shower simulation is shown in Fig. 8. Below Pf $= 0.4$, where matrix-element events are discarded due to the infrared cutoff, we see that hadronization affects the shape of the jet function significantly. Above this value, hadronization affects only the overall normalization.

B. Estimation of noncollinear corrections

Our theoretical computation relies on two approximations. The first is working to leading order in perturbation theory, which is valid for sizable mass and planar flow, well above the peak locations in the resummed distributions.

[9] In SHERPA, the CKKW matching scale Q_{cut} also serves as this cutoff.

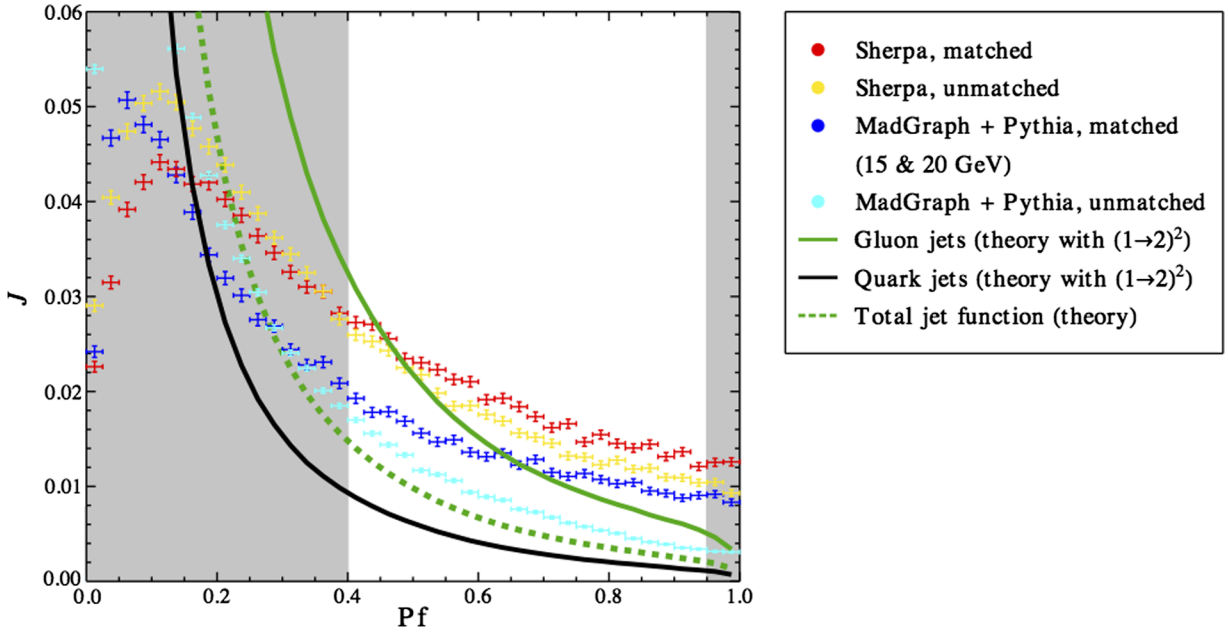

FIG. 7 (color online). Comparison of jet functions from parton-shower simulations and semianalytic results using a strong-ordering approximation (iterated $1 \to 2$ splitting functions). The two factors of the strong coupling α_s are evaluated at the jet-mass scale and the scale of the second splitting s_{ij}. The region of expected validity of the semianalytic form is highlighted. The curves and points are as in Fig. 5.

The validity of this approximation requires that resummation effects be negligible, $\alpha_s(m)\log(m/pR) \ll 1$ and $\alpha_s(m)\log \mathrm{Pf} \ll 1$, for m and Pf, respectively. It also requires that the values of these variables not be too close to kinematic boundaries, such as $m = pR$ and $\mathrm{Pf} = 1$. The second approximation is the collinear approximation, valid for narrow jets. The two approximations limit the region of validity, while offering a nontrivial window of applicability for the calculations. The window is home to a variety of potential new-physics searches, for example those using boosted top-quark jets.

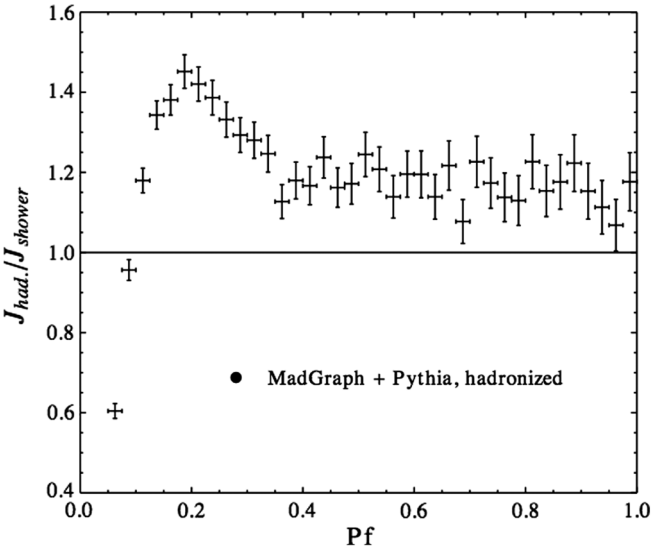

FIG. 8. A comparison of parton-shower jet functions with and without hadronization, shown as a ratio of the two. Both distributions are from MADGRAPH+PYTHIA simulations with matched jets.

We would like to have a better understanding of the corrections to our theoretical results, and accordingly we would like to separate the collinear corrections from those due to resummation. For that purpose we consider a matrix-element calculation, with no showering or hadronization, and compare it with our theoretical prediction (see Fig. 9). This calculation is carried out at leading order in α_s, and thus differs from our theoretical prediction only in corrections to the collinear approximation, as the tree-level matrix elements employed are exact throughout phase space. The difference between the two results provides an estimation of the corrections away from the $R \to 0$ limit. We see in Fig. 9 that these corrections vary significantly with Pf.

We normalize the exact leading-order jet function $J_f^{(e)}$ to match the way the semianalytic jet function is normalized at leading order ($\mathcal{O}(\alpha_s^2)$), so that

$$\int dm^2 J_f^{(e)} = \left(\int dp_{\mathrm{T}} d\eta \frac{d\sigma_{2\to f,x}}{dp_{\mathrm{T}} d\eta}\right)^{-1} \times \int dp_{\mathrm{T}} d\eta dm^2 \frac{d\sigma_{2\to J,x}}{dp_{\mathrm{T}} d\eta dm^2 d\mathrm{Pf}}. \quad (63)$$

Here, $\sigma_{2\to f,x}$ is the $2 \to 2$ cross section (x denotes a parton of any flavor), and $\sigma_{2\to J,x}$ is the $2 \to 4$ cross section for an outgoing state that includes a jet J of matching type. Both cross sections are computed to leading order in α_s. The integrals are over the window $950 < p_{\mathrm{T}} < 1050$ GeV,

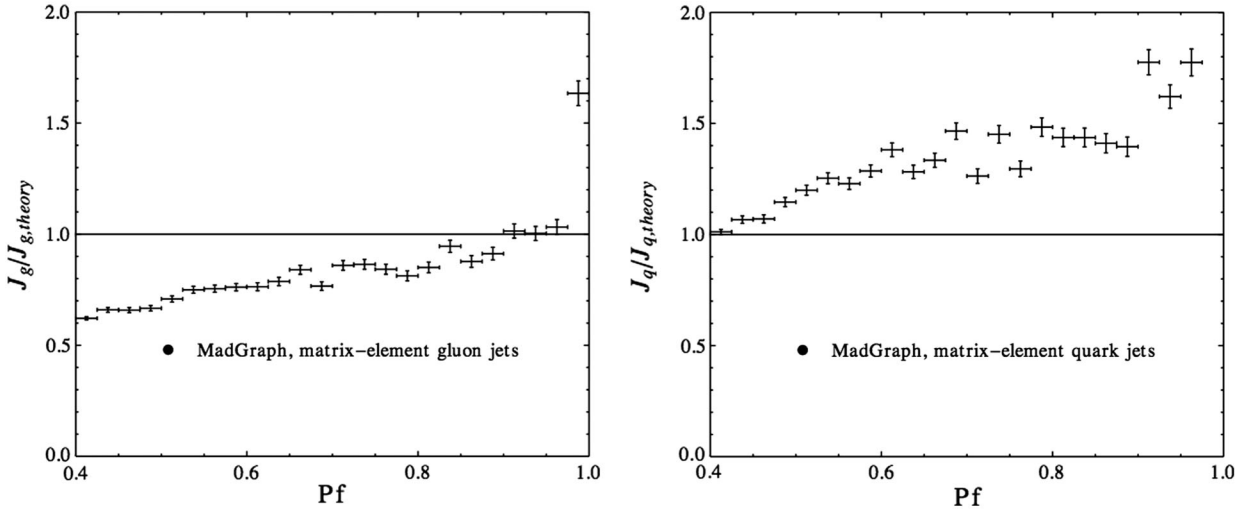

FIG. 9. Comparison of gluon and quark semianalytic jet functions, with the results from MADGRAPH matrix-element $2 \to 4$ calculations. The parameters are $p = 1$ TeV, $m = 180$ GeV, and $R = 0.4$.

$|\eta| < 1$ and $160 < m < 200$ GeV, with the jet function itself evaluated at $p_T = 1$ TeV.

Let us relate these objects to quantities that are directly measurable in a Monte Carlo integration. Consider the differential cross section $d\sigma$ in a given bin, for example the cross section for events within our kinematic window, and with planar flow in a small range $[\mathrm{Pf}, \mathrm{Pf} + d\mathrm{Pf})$. It is given by

$$d\sigma = \frac{dN}{N}\sigma, \tag{64}$$

where dN is the number of events inside the bin, N is the total number of events produced in the integration, and σ is the total cross section computed by the simulation. Using this relation in Eq. (63), we find that the jet function is given by

$$\int dm^2 J_f(\mathrm{Pf}) = \frac{1}{d\mathrm{Pf}} \frac{N_{2\to 2}}{N_{2\to 4}} \frac{\sigma_{2\to 4}}{\sigma_{2\to 2}} \frac{\tilde{N}_{2\to J,x}(\mathrm{Pf})}{\tilde{N}_{2\to f,x}}. \tag{65}$$

Here, $N_{2\to X}$ and $\sigma_{2\to X}$ are the total number of events and total cross section produced in the $2 \to X$ simulation; $\tilde{N}_{2\to f,x}$ is the total number of events in the $2 \to 2$ integration, with a parton of flavor f, that fall within our kinematic window; and $\tilde{N}_{2\to J,x}$ is the total number of events in the $2 \to 4$ integration, with a jet of flavor f, that fall within our kinematic window (including jet mass), and within our Pf bin.

VII. CONCLUSIONS

The Pf distribution of highly boosted narrow massive jets is interesting, because a nonvanishing value of this variable implies that the corresponding jet consists of at least three hard partons in a perturbative description. QCD jets with sizable planar flow and jet mass (m) form an important background to various new-physics signals. For instance, massive jets with large Pf arise in models with heavy resonances decaying dominantly to top quarks or in supersymmetric models with R-parity-violating gluinos. In this paper, we have studied the planar flow distribution of narrow QCD jets. We obtained a semianalytic form for this distribution, independent of the underlying hard process giving rise to the jet. We have made use of QCD factorization properties to do so, and have computed jet functions which express the probability of a parent parton fragmenting into a jet of given planar flow and mass. We computed the leading-order approximation to these jet functions using the universal $1 \to 3$ tree-level collinear splitting functions. We compared this approximation to a strongly ordered collinear approximation, using iterated $1 \to 2$ splitting functions, and find substantial differences. Our results are, unsurprisingly, sensitive to the choice of scales in the strong coupling. We have also derived the leading-log behavior of the jet functions analytically. Our results are expected to be valid only in the range $0.4 \lesssim \mathrm{Pf} \lesssim 0.95$, and for sizable jet mass, as fixed-order predictions will diverge both as $\mathrm{Pf} \to 0$ and $m \to 0$. The divergence of the planar-flow distribution should be regulated by resummation of leading logarithms to all orders in perturbation theory. To the best of our knowledge, this resummation has not been computed, and the resulting resummed distribution would be of interest.

We have compared our semianalytic jet function to parton-shower predictions using various event generators. The broad features are in agreement in the region of validity of our fixed-order calculation, as the parton-shower results interpolate between the predicted quark and gluon jet functions. The details differ, however, between the parton-shower results and a suitably-weighted

average of quark and gluon jet functions. We find that the results from SHERPA are above our semianalytic calculations, both with and without matching (using CKKW). In contrast, the results from MADGRAPH with PYTHIA showering are above our results with matching (using MLM), but below our predictions without matching. In the region of validity, hadronization effects increase the value of the jet function modestly without altering its shape. We note that the results of these two parton-shower codes do not agree with each other, either with or without matching. The differences between them, even with matching, are comparable to the differences from our semianalytic results, and the differences are greater without matching. This variation suggests that some caution should be exercised when comparing these results with experimental data, and that a data-driven approach to jet substructure should be explored as well. The qualitative agreement of the semianalytic results with the parton-shower calculations does however suggest that further refinement of the fixed-order prediction, for example by carrying out a next-to-leading order calculation, would be valuable. The required $2 \to 4$ one-loop matrix elements are available, and have already been used for phenomenological studies [48,49].

Planar flow is one of several three-prong substructure variables that can play a role in discriminating highly boosted jets arising from three-body decays of heavy particles from QCD backgrounds. It tends to be sensitive to soft radiation near the edge of the jet, which also makes it sensitive to pileup. This motivates the use of jet filtering or template overlaps, where the hard substructure in a jet can be enhanced in a controlled manner. Such enhancement would be expected to bring jet functions closer to the fixed-order perturbative ones calculated in this paper.

ACKNOWLEDGMENTS

It is a pleasure to thank Johan Alwall, Frank Krauss, and Gavin Salam for useful discussions. The figures for this article have been created using the LevelScheme scientific figure preparation system [55]. M. F. would like to thank the Weizmann Institute of Science for support while most of this work was carried out. The research of D. A. K. is supported by the European Research Council under Advanced Investigator Grant No. ERC-AdG-228301. G. P. is supported by grants from the Gruber foundation, IRG, ISF, and Minerva.

APPENDIX A: $1 \to 2$ SPLITTING FUNCTIONS

In this section, for completeness, we quote the $1 \to 2$ spin-averaged and color-averaged splitting functions [32,37] $P_{f_1 f_2}$ at leading order in α_s. Let us define

$$C_F = \frac{N_c^2 - 1}{2N_c}, \qquad C_A = N_c, \qquad T_R = \frac{1}{2}. \tag{A1}$$

The functions are

$$P_{qg}(z) = C_F \frac{1 + (z-1)^2}{z}, \tag{A2}$$

$$P_{q\bar{q}}(z) = T_R[1 - 2z(1-z)], \tag{A3}$$

$$P_{gg}(z) = 2C_A\left[\frac{z}{1-z} + \frac{1-z}{z} + z(1-z)\right], \tag{A4}$$

and the rest are determined by charge conjugation; for example, $P_{qg} = P_{\bar{q}g}$.

APPENDIX B: $1 \to 3$ SPLITTING FUNCTIONS

In this section we write down the $1 \to 3$ spin-averaged and color-averaged splitting functions $P_{f_1 f_2 f_3}$ at leading order in α_s. We follow the conventions of Ref. [37]. Our definition of z_i agrees with this reference in the collinear limit. In addition to Eq. (A1), we define

$$t_{ij,k} \equiv 2\frac{z_i s_{jk} - z_j s_{ik}}{z_i + z_j} + \frac{z_i - z_j}{z_i + z_j} s_{ij}. \tag{B1}$$

Quark splitting to quarks.—

$$P_{\bar{Q}_1 Q_2 q_3} = \frac{1}{2} C_F T_R \frac{s_{123}}{s_{12}}\left[-\frac{t_{12,3}^2}{s_{12}s_{123}} + \frac{4z_3 + (z_1 - z_2)^2}{z_1 + z_2} + z_1 + z_2 - \frac{s_{12}}{s_{123}}\right], \tag{B2}$$

$$P_{\bar{q}_1 q_2 q_3} = [P_{\bar{Q}_1 Q_2 q_3} + (2 \leftrightarrow 3)] + P^{(\mathrm{id})}_{\bar{q}_1 q_2 q_3}, \tag{B3}$$

where

$$P^{(\mathrm{id})}_{\bar{q}_1 q_2 q_3} = C_F\left(C_F - \frac{1}{2}C_A\right)\left\{\frac{2s_{23}}{s_{12}} + \frac{s_{123}}{s_{12}}\left(\frac{1+z_1^2}{1-z_2} - \frac{2z_2}{1-z_3}\right) - \frac{s_{123}^2}{s_{12}s_{13}}\frac{z_1}{2}\left[\frac{1+z_1^2}{(1-z_2)(1-z_3)}\right]\right\} + (2 \leftrightarrow 3). \tag{B4}$$

Quark splitting to quark+gluons.—

$$P_{g_1 g_2 q_3} = C_F^2 P^{(\mathrm{ab})}_{g_1 g_2 q_3} + C_F C_A P^{(\mathrm{nab})}_{g_1 g_2 q_3}, \tag{B5}$$

where

$$P^{(\mathrm{ab})}_{g_1 g_2 q_3} = \left\{\frac{s_{123}^2}{2s_{13}s_{23}}\frac{z_3(1+z_3^2)}{z_1 z_2} + \frac{s_{123}}{s_{13}}\left[\frac{z_3(1-z_1) + (1-z_2)^3}{z_1 z_2}\right] - \frac{s_{23}}{s_{13}}\right\} + (1 \leftrightarrow 2), \tag{B6}$$

$$P^{(\mathrm{nab})}_{g_1g_2q_3} = \left\{\frac{t^2_{12,3}}{4s^2_{12}} + \frac{1}{4} + \frac{s^2_{123}}{2s_{12}s_{13}}\left[\frac{(1-z_3)^2+2z_3}{z_2} + \frac{z_2^2+2(1-z_2)}{1-z_3}\right] - \frac{s^2_{123}}{4s_{13}s_{23}}z_3\left[\frac{(1-z_3)^2+2z_3}{z_1z_2}\right]\right.$$
$$+ \frac{s_{123}}{2s_{12}}\left[\frac{z_1(2-2z_1+z_1^2)-z_2(6-6z_2+z_2^2)}{z_2(1-z_3)}\right] + \frac{s_{123}}{2s_{13}}\left[\frac{(1-z_2)^3+z_3^2-z_2}{z_2(1-z_3)} - \frac{z_3(1-z_1)+(1-z_2)^3}{z_1z_2}\right]\Bigg\}$$
$$+ (1 \leftrightarrow 2). \tag{B7}$$

Gluon splitting to gluon+quarks.—

$$P_{g_1q_2\bar{q}_3} = C_F T_R P^{(\mathrm{ab})}_{g_1q_2\bar{q}_3} + C_A T_R P^{(\mathrm{nab})}_{g_1q_2\bar{q}_3}, \tag{B8}$$

where

$$P^{(\mathrm{ab})}_{g_1q_2\bar{q}_3} = -2 - s_{23}\left(\frac{1}{s_{12}} + \frac{1}{s_{13}}\right) + 2\frac{s^2_{123}}{s_{12}s_{13}}[1 - z_1(1-z_1) - 2z_2z_3] - \frac{s_{123}}{s_{12}}(1-2z_2) - \frac{s_{123}}{s_{13}}(1-2z_3), \tag{B9}$$

$$P^{(\mathrm{nab})}_{g_1q_2\bar{q}_3} = \left\{-\frac{t^2_{23,1}}{4s^2_{23}} + \frac{s^2_{123}}{2s_{13}s_{23}}z_3\left[\frac{(1-z_1)^3-z_1^3}{z_1(1-z_1)} - \frac{2z_3(1-z_3-2z_1z_2)}{z_1(1-z_1)}\right] + \frac{s_{123}}{2s_{13}}(1-z_2)\left[1 + \frac{1}{z_1(1-z_1)} - \frac{2z_2(1-z_2)}{z_1(1-z_1)}\right]\right.$$
$$\left. + \frac{s_{123}}{2s_{23}}\left[\frac{1+z_1^3}{z_1(1-z_1)} + \frac{z_1(z_3-z_2)^2 - 2z_2z_3(1+z_1)}{z_1(1-z_1)}\right] - \frac{1}{4} - \frac{s^2_{123}}{2s_{12}s_{13}}[1 - z_1(1-z_1) - 2z_2z_3]\right\} + (2 \leftrightarrow 3). \tag{B10}$$

Gluon splitting to gluons.—

$$P_{g_1g_2g_3} = C_A^2\left\{\frac{t^2_{12,3}}{4s^2_{12}} + \frac{3}{4} + \frac{s_{123}}{s_{12}}\left[4\frac{z_1z_2-1}{1-z_3} + \frac{z_1z_2-2}{z_3} + \frac{3}{2} + \frac{5}{2}z_3 + \frac{(1-z_3(1-z_3))^2}{z_3z_1(1-z_1)}\right]\right.$$
$$\left. + \frac{s^2_{123}}{s_{12}s_{13}}\left[\frac{z_1z_2(1-z_2)(1-2z_3)}{z_3(1-z_3)} + z_2z_3 - 2 + \frac{z_1(1+2z_1)}{2} + \frac{1+2z_1(1+z_1)}{2(1-z_2)(1-z_3)} + \frac{1-2z_1(1-z_1)}{2z_2z_3}\right]\right\}$$
$$+ (5\,\text{permutations}). \tag{B11}$$

APPENDIX C: THREE-PARTON KINEMATICS IN THE NARROW-JET APPROXIMATION

In this Appendix we write down kinematic quantities of three-parton configurations, at leading order in the collinear approximation $\theta_i \le R \ll 1$, in terms of the integration variables of Eq. (33). As dictated by the kinematics we assume $m < pR$ [see Eq. (35)], and this implies that $m \ll p$.

For parton three-momenta we use spherical coordinates (p_i, θ_i, ϕ_i) with $i = 1, 2, 3$, relative to the jet axis $\vec{p}$, and we define $\phi \equiv \phi_1 - \phi_2$. In the collinear approximation,

$$E = p + \frac{m^2}{2p} + o(R^4), \tag{C1}$$

$$z_i = \frac{p_i}{p}\left(1 - \frac{m^2}{2p^2}\right) + o(R^4), \tag{C2}$$

$$s_{ij} = p_ip_j\theta_{ij}^2 + o(R^4) = z_iz_jp^2\theta_{ij}^2 + o(R^4), \tag{C3}$$

where θ_{ij} is the angle between partons i and j.

For parton 3, we have

$$p_3 = \sqrt{(p-p_1-p_2)^2 + p(p_1\theta_1^2 + p_2\theta_2^2) - p_1p_2\theta_{12}^2} + o(R^4)$$
$$= |p - p_1 - p_2| + \frac{p(p_1\theta_1^2 + p_2\theta_2^2) - p_1p_2\theta_{12}^2}{2|p-p_1-p_2|} + o(R^4), \tag{C4}$$

$$\theta_3^2 = \frac{1}{|p-p_1-p_2|}\left[\frac{m^2}{p} - p_1\theta_1^2 - p_2\theta_2^2\right] + o(R^4). \tag{C5}$$

In expanding the square root in p_3 we assumed that $p - p_1 - p_2$ is large relative to the second term. This assumption in not valid in the limit of soft p_3, where in fact $p - p_1 - p_2$ becomes arbitrarily small (and even negative). To avoid this limit we restrict ourselves to the range $p_1 < p_2, p_3$.

The angles θ_{ij} are given by

$$\theta_{12}^2 = \theta_1^2 + \theta_2^2 - 2\theta_1\theta_2\cos\phi + o(R^4), \tag{C6}$$

$$\theta_{13}^2 = \frac{1}{p - p_1 - p_2}\left[\frac{m^2}{p} + p\theta_1^2 - p_2\theta_{12}^2\right] + o(R^4), \tag{C7}$$

$$\theta_{23}^2 = \frac{1}{p - p_1 - p_2}\left[\frac{m^2}{p} + p\theta_2^2 - p_1\theta_{12}^2\right] + o(R^4). \tag{C8}$$

Finally, for the jet mass and planar flow we have

$$m^2 = p\sum_{i=1}^{3} p_i\theta_i^2 + o(R^4) = \frac{p}{p - p_1 - p_2}[p(p_1\theta_1^2 + p_2\theta_2^2) - p_1p_2\theta_{12}^2] + o(R^4), \tag{C9}$$

$$\mathrm{Pf} = \frac{4p^3p_1p_2\theta_1^2\theta_2^2\sin^2\phi}{m^4(p - p_1 - p_2)} + o(R^2). \tag{C10}$$

APPENDIX D: ANALYTIC LEADING-LOG COEFFICIENTS

In this section we write down the coefficients A_f of the leading-log jet function (48), computed analytically from the integral (47). We find

$$A_g = \frac{2\alpha_s^2C_A^2}{\pi^2}\frac{1}{m^2}\log\left(\frac{p^2R^2}{m^2}\right) + \frac{\alpha_s^2}{6\pi^2}\frac{(11C_A^2 - 4T_RN_fC_F)(m^6 - p^6R^6) + 9C_A^2m^2p^2R^2(m^2 - p^2R^2)}{m^2(m^2 + p^2R^2)^3}, \tag{D1}$$

$$A_q = \frac{\alpha_s^2C_F(C_A + C_F)}{\pi^2}\frac{1}{m^2}\log\left(\frac{p^2R^2}{m^2}\right) + \frac{3\alpha_s^2C_F(C_A + C_F)}{4\pi^2}\frac{m^2 - p^2R^2}{m^2(m^2 + p^2R^2)}. \tag{D2}$$

The constants C_A, C_F, and T_R are defined in Eq. (A1).

APPENDIX E: STRONG COUPLING RENORMALIZATION SCALES

In this section we explain in detail our choice of running scale μ for the second factor of α_s that appears in the jet function (33). The first factor, corresponding to the first $1 \to 2$ splitting, is evaluated at the jet-mass scale. To make a realistic choice for μ (which corresponds to the scale of the second $1 \to 2$ splitting), we use the dipole model [50–54], in which a $2 \to 3$ splitting of partons is described as an emission from a color dipole consisting of the two parent partons. The natural scale for this process is given by[10]

$$\mu^2 = \frac{s_{12}s_{23}}{s_{123}} \tag{E1}$$

in the case where partons 1 and 3 form the dipole, and parton 2 is being emitted. In our case we do not know which of the partons is emitted in the second splitting, and in fact the second splitting is not even well defined in general. We choose the scale to be the minimal one among the several options (corresponding to permutations of the partons), relying on the splitting function's preference for soft-collinear emissions. For example, in the case of $g \to ggg$ splitting, the scale is given by

$$\mu^2_{g\to ggg} = \min_{i,j,k}\left\{\frac{s_{ij}s_{jk}}{s_{123}}\right\}. \tag{E2}$$

The dipole model does not describe cases where the second splitting process is quark-pair production, and in such cases we choose μ to be the mass of the produced pair. The scales for the remaining processes are given by

$$\mu^2_{g\to g_1q_2\bar{q}_3} = \min\left\{\frac{s_{12}s_{13}}{s_{123}}, s_{23}\right\}, \tag{E3}$$

$$\mu^2_{q\to g_1g_2q_3} = \min\left\{\frac{s_{12}s_{23}}{s_{123}}, \frac{s_{12}s_{13}}{s_{123}}\right\}, \tag{E4}$$

$$\mu^2_{q\to \bar{q}_1q_2q_3} = \min\{s_{12}, s_{13}\}, \tag{E5}$$

$$\mu^2_{q\to \bar{Q}_1Q_2q_3} = s_{12}. \tag{E6}$$

APPENDIX F: MASS AND PLANAR-FLOW LEADING-ORDER JET FUNCTIONS FROM SPLITTING FUNCTIONS

In this Appendix we consider the jet function's behavior in the limit of small planar flow, basically using an iterated $1 \to 2$ splitting analysis in the limit of strong ordering. Let us first examine in more detail how one can obtain the jet-mass distribution in the soft-collinear limit: the single emission rate is proportional to

$$d\sigma_{1\to 2}(z, \theta) \propto \frac{dz}{z}\frac{d\theta}{\theta}, \tag{F1}$$

[10] In the limit of soft-collinear emission, μ becomes the p_T of the emitted parton relative to its parent.

where z is the energy fraction of the emitted gluon and θ is the angle between the emitted gluon and the parent parton. In this approximation the jet mass is

$$m_J^2 = E^2 z\theta^2. \tag{F2}$$

For a fixed emission angle, θ, we can rewrite Eq. (F1) as

$$d\sigma(m_J^2, \theta) \propto \frac{dm_J^2}{m_J^2}\frac{d\theta}{\theta}, \tag{F3}$$

where now $R^2 > \theta^2 > m_J^2/E^2$. We see that for a fixed mass, the distribution of θ is characterized by $1/\theta$. The jet-mass distribution is obtained upon integrating θ between the boundaries of integration, giving

$$\frac{d\sigma_{1\to 2}}{dm_J^2} \propto \frac{1}{m_J^2}\log\left(\frac{R^2E^2}{m_J^2}\right), \tag{F4}$$

where in hadronic collisions E should be replaced by p_T. The missing proportionality coefficient is nothing but $\alpha_s C_A/\pi$ (for a gluon jet).

Next let us try to obtain an expression for the planar-flow distribution in the limit of small planar flow for a massive jet. In this limit, we expect that the dominant contribution arises from configurations where the third parton is soft and collinear to either of the first two partons. This contribution should be described well by a $1 \to 2$ splitting function. We can thus iterate the above expression starting with a two parton configuration of mass m_J where the two patrons are separated by an angle $\sim\theta$. We can now add a second emission with an angle θ' such that $\theta' \ll \theta$ and an energy fraction $z' \ll z$ such that the third parton can be thought as soft and collinear with respect to either of the first two partons. The differential cross section describing this configuration is given by

$$d\sigma(m_J^2, \theta) \times d\sigma_{1\to 2}(\theta', z') \propto \frac{dm_J^2}{m_J^2}\frac{d\theta}{\theta} \times \frac{dz'}{z'}\frac{d\theta'}{\theta'}, \tag{F5}$$

where now z' is integrated between 0 and $z/2$ at most. (At the upper boundary, both partons have the same energy; this violates the soft approximation but is highly suppressed due to the weight in the splitting function.) Likewise, θ' is integrated between 0 and θ at most. For a fixed value of mass and planar flow z' and θ' are not really independent to leading order. The tensor $\mathcal{I}$ describing this configuration is

$$\mathcal{I} = E\begin{pmatrix} [z, (1-z)]z'\theta'^2\sin^2\phi & [z\theta_s, (1-z)(1-\theta_s)]z'\theta'\sin 2\phi/2 \\ [z\theta_s, (1-z)(1-\theta_s)]z'\theta'\sin 2\phi/2 & (1-z)(\theta-\theta_s)^2 + z\theta_s^2 \end{pmatrix}. \tag{F6}$$

It is easy to check that $\theta_s = (1-z)\theta$ and $(1-z)\times(\theta-\theta_s)^2 + z\theta_s^2 = z(1-z)\theta^2 = m^2/E^2$, and the bracketed expressions in the (11, 12, 21) entries cover the cases where the third parton is emitted from the harder or softer of the first two patrons, the softer one being characterized by an angle $\theta_s = (1-z)\theta$. ϕ describes the azimuthal angle—the third parton's emission angle relative to the line connecting the two hard partons. To leading order in z' we find

$$\mathrm{Pf} = 4\frac{E^2}{m^2}[z, (1-z)]z'\theta'^2\sin^2\phi \approx 4\frac{E^2}{m^2}z'\theta'^2\sin^2\phi, \tag{F7}$$

where on the right-hand side of the above relation we have focused on the most singular region $z' \ll z \ll 1$. Similarly to the jet-mass case we can interchange z' and Pf in the singular region, $\mathrm{Pf} \ll 1$. Integrating over the first emission and using the splitting function for both radiations (assuming only gluons for simplicity), focusing on the most singular region $z' \ll z \ll 1$, $\theta' \ll \theta \ll 1$ and changing variables from z' to Pf (we can ignore ϕ as in this approximation the splitting function does not depend on it), we find

$$\left.\frac{d^3\sigma}{dm d\mathrm{Pf} d\theta'}\right|_{\mathrm{Pf}\ll 1} \approx \frac{\alpha_s C_A}{\pi m_J^2}\log\left(\frac{R^2E^2}{m_J^2}\right) \times \frac{\alpha_s C_A}{\pi}\frac{1}{\mathrm{Pf}}\frac{1}{\theta'}. \tag{F8}$$

For a given Pf the range for θ' is

$$\sqrt{\mathrm{Pf}}\frac{2m}{E} \ll \theta' \ll R. \tag{F9}$$

Integrating over θ' yields the final expression for the Pf distribution for jets of small Pf and mass,

$$\left(\frac{d^2\sigma}{d\mathrm{Pf} dm}\right)_{\mathrm{Pf}\ll 1} \approx \frac{\alpha_s^2 C_A^2}{\pi^2 m_J^2}\log\left(\frac{R^2E^2}{m_J^2}\right) \times \frac{1}{\mathrm{Pf}}\log\left(\frac{ER}{2m\sqrt{\mathrm{Pf}}}\right), \tag{F10}$$

where in hadronic collisions E should be replaced with p_T.

[1] G. Aad *et al.* (ATLAS Collaboration), J. High Energy Phys. 09 (2012) 041; Phys. Lett. B **718**, 1284 (2013); J. High Energy Phys. 01 (2013) 116.

[2] S. Chatrchyan *et al.* (CMS Collaboration), J. High Energy Phys. 12 (2012) 015; 09 (2012) 029; CMS Collaboration, Report No. EXO-11-006.

[3] G. Aad *et al.* (ATLAS Collaboration), Phys. Rev. D **86**, 072006 (2012); J. High Energy Phys. 05 (2012) 128.

[4] S. Rappoccio *et al.* (CMS Collaboration), AIP Conf. Proc. **1441**, 820 (2012); CMS Collaboration, Report No. CMS-PAS-JME-10-013.

[5] T. Aaltonen *et al.* (CDF Collaboration), Phys. Rev. D **85**, 091101 (2012); Report No. CDF/ANAL/TOP/PUBLIC/10234.

[6] J. M. Butterworth, B. E. Cox, and J. R. Forshaw, Phys. Rev. D **65**, 096014 (2002).

[7] K. Agashe, A. Belyaev, T. Krupovnickas, G. Perez, and J. Virzi, Phys. Rev. D **77**, 015003 (2008).

[8] B. Lillie, L. Randall, and L.-T. Wang, J. High Energy Phys. 09 (2007) 074.

[9] J. M. Butterworth, A. R. Davison, M. Rubin, and G. P. Salam, Phys. Rev. Lett. **100**, 242001 (2008).

[10] J. M. Butterworth, J. R. Ellis, A. R. Raklev, and G. P. Salam, Phys. Rev. Lett. **103**, 241803 (2009).

[11] J. M. Butterworth, J. R. Ellis, and A. R. Raklev, J. High Energy Phys. 05 (2007) 033.

[12] S. D. Ellis, J. Huston, K. Hatakeyama, P. Loch, and M. Tonnesmann, Prog. Part. Nucl. Phys. **60**, 484 (2008).

[13] A. Abdesselam, E. B. Kuutmann, U. Bitenc, G. Brooijmans, J. Butterworth, P. Bruckman de Renstrom, D. B. Franzosi, R. Buckingham *et al.*, Eur. Phys. J. C **71**, 1661 (2011); A. Altheimer, S. Arora, L. Asquith, G. Brooijmans, J. Butterworth, M. Campanelli, B. Chapleau, A. E. Cholakian *et al.*, J. Phys. G **39**, 063001 (2012).

[14] G. P. Salam, Eur. Phys. J. C **67**, 637 (2010).

[15] P. Nath, B. D. Nelson, H. Davoudiasl, B. Dutta, D. Feldman, Z. Liu, T. Han, P. Langacker *et al.*, Nucl. Phys. B, Proc. Suppl. **200–202**, 185 (2010).

[16] L. G. Almeida, R. Alon, and M. Spannowsky, Eur. Phys. J. C **72**, 2113 (2012); A. J. Buras, G. Perez, T. A. Schwarz, and T. M. P. Tait, Eur. Phys. J. C **72**, 2105 (2012); T. Plehn and M. Spannowsky, J. Phys. G **39**, 083001 (2012).

[17] G. Gur-Ari, M. Papucci, and G. Perez, arXiv:1101.2905.

[18] L. G. Almeida, S. J. Lee, G. Perez, G. F. Sterman, I. Sung, and J. Virzi, Phys. Rev. D **79**, 074017 (2009).

[19] L. G. Almeida, S. J. Lee, G. Perez, G. Sterman, and I. Sung, Phys. Rev. D **82**, 054034 (2010).

[20] C. F. Berger, T. Kucs, and G. F. Sterman, Phys. Rev. D **68**, 014012 (2003).

[21] G. Brooijmans *et al.* (New Physics Working Group Collaboration), arXiv:1005.1229; Y. Eshel, O. Gedalia, G. Perez, and Y. Soreq, Phys. Rev. D **84**, 011505 (2011).

[22] L. G. Almeida, S. J. Lee, G. Perez, I. Sung, and J. Virzi, Phys. Rev. D **79**, 074012 (2009).

[23] J. Thaler and L.-T. Wang, J. High Energy Phys. 07 (2008) 092.

[24] M. Cacciari, G. P. Salam, and G. Soyez, J. High Energy Phys. 04 (2008) 005.

[25] D. Krohn, J. Shelton, and L.-T. Wang, J. High Energy Phys. 07 (2010) 041.

[26] G. Soyez, G. P. Salam, J. Kim, S. Dutta, and M. Cacciari, arXiv:1211.2811; R. Alon, E. Duchovni, G. Perez, A. P. Pranko, and P. K. Sinervo, Phys. Rev. D **84**, 114025 (2011); S. Sapeta, Q. C. Zhang, and Q. C. Zhang, J. High Energy Phys. 06 (2011) 038.

[27] D. Krohn, J. Thaler, and L.-T. Wang, J. High Energy Phys. 02 (2010) 084; S. D. Ellis, C. K. Vermilion, and J. R. Walsh, Phys. Rev. D **81**, 094023 (2010).

[28] J. Thaler and K. Van Tilburg, J. High Energy Phys. 02 (2012) 093; C. Chen, Phys. Rev. D **85**, 034007 (2012); Z. Han, Phys. Rev. D **86**, 014026 (2012); I. Feige, M. Schwartz, I. Stewart, and J. Thaler, Phys. Rev. Lett. **109**, 092001 (2012); G. Brooijmans, Report No. ATL-PHYS-CONF-2008-008; T. Plehn, G. P. Salam, and M. Spannowsky, Phys. Rev. Lett. **104**, 111801 (2010); T. Plehn, M. Spannowsky, and M. Takeuchi, Phys. Rev. D **85**, 034029 (2012); J. High Energy Phys. 05 (2011) 135.

[29] J. Thaler and K. Van Tilburg, J. High Energy Phys. 03 (2011) 015; Y. Cui, Z. Han, and M. D. Schwartz, Phys. Rev. D **83**, 074023 (2011); C. Delaunay, O. Gedalia, S. J. Lee, G. Perez, and E. Ponton, Phys. Lett. B **703**, 486 (2011).

[30] A. Hook, M. Jankowiak, and J. G. Wacker, J. High Energy Phys. 04 (2012) 007; D. E. Soper and M. Spannowsky, Phys. Rev. D **84**, 074002 (2011); arXiv:1211.3140; M. Jankowiak and A. J. Larkoski, J. High Energy Phys. 06 (2011) 057; S. D. Ellis, C. K. Vermilion, J. R. Walsh, A. Hornig, and C. Lee, J. High Energy Phys. 11 (2010) 101; A. Banfi, M. Dasgupta, K. Khelifa-Kerfa, and S. Marzani, J. High Energy Phys. 08 (2010) 064; D. E. Kaplan, K. Rehermann, M. D. Schwartz, and B. Tweedie, Phys. Rev. Lett. **101**, 142001 (2008).

[31] A. Hornig, C. Lee, and G. Ovanesyan, J. High Energy Phys. 05 (2009) 122; D. Krohn, J. Thaler, and L.-T. Wang, J. High Energy Phys. 06 (2009) 059; S. D. Ellis, C. K. Vermilion, and J. R. Walsh, Phys. Rev. D **80**, 051501 (2009); C. Lee, A. Hornig, and G. Ovanesyan, Proc. Sci. EFT09 (2009) 010 [arXiv:0905.0168]; M. Cacciari, arXiv:0906.1598.

[32] G. Altarelli and G. Parisi, Nucl. Phys. **B126**, 298 (1977).

[33] G. F. Sterman, arXiv:hep-ph/0412013.

[34] I. M. Dremin, AIP Conf. Proc. **828**, 30 (2006).

[35] T. Han, arXiv:hep-ph/0508097.

[36] G. F. Sterman, arXiv:hep-ph/9606312.

[37] S. Catani and M. Grazzini, Phys. Lett. B **446**, 143 (1999).

[38] M. E. Peskin and D. V. Schroeder, *An Introduction to Quantum Field Theory* (Addison-Wesley, Reading, MA, 1995).

[39] J. M. Campbell and E. W. N. Glover, Nucl. Phys. **B527**, 264 (1998).

[40] S. Catani, L. Trentadue, G. Turnock, and B. R. Webber, Nucl. Phys. **B407**, 3 (1993).

[41] J. Alwall, M. Herquet, F. Maltoni, O. Mattelaer, and T. Stelzer, J. High Energy Phys. 06 (2011) 128.

[42] T. Sjostrand, S. Mrenna, and P. Z. Skands, J. High Energy Phys. 05 (2006) 026.

[43] T. Gleisberg, S. Hoeche, F. Krauss, M. Schonherr, S. Schumann, F. Siegert, and J. Winter, J. High Energy Phys. 02 (2009) 007.

[44] J. Pumplin, D. R. Stump, J. Huston, H. L. Lai, P. M. Nadolsky, and W. K. Tung, J. High Energy Phys. 07 (2002) 012.
[45] G. P. Salam and G. Soyez, J. High Energy Phys. 05 (2007) 086.
[46] M. Cacciari, G. P. Salam, and G. Soyez, Eur. Phys. J. C **72**, 1896 (2012).
[47] M. Cacciari and G. P. Salam, Phys. Lett. B **641**, 57 (2006).
[48] Z. Bern, G. Diana, L. J. Dixon, F. F. Cordero, S. Hoeche, D. A. Kosower, H. Ita, D. Maître, and K. Ozeren, Phys. Rev. Lett. **109**, 042001 (2012).
[49] S. Badger, B. Biedermann, P. Uwer, and V. Yundin, Phys. Lett. B **718**, 965 (2013).
[50] G. Gustafson, Phys. Lett. B **175**, 453 (1986).
[51] G. Gustafson and U. Pettersson, Nucl. Phys. **B306**, 746 (1988).
[52] W. T. Giele, D. A. Kosower, and P. Z. Skands, Phys. Rev. D **78**, 014026 (2008).
[53] W. T. Giele, D. A. Kosower, and P. Z. Skands, Phys. Rev. D **84**, 054003 (2011).
[54] J.-C. Winter and F. Krauss, J. High Energy Phys. 07 (2008) 040.
[55] M. A. Caprio, Comput. Phys. Commun. **171**, 107 (2005).